nature

https://doi.org/10.1038/s41586-022-05609-w

Accelerated Article Preview

Antibody feedback regulates immune memory after SARS-CoV-2 mRNA vaccination

Received: 4 June 2022

Accepted: 30 November 2022

Accelerated Article Preview

Cite this article as: Schaefer-Babajew, D. et al. Antibody feedback regulates immune memory after SARS-CoV-2 mRNA vaccination. *Nature* https://doi.org/10.1038/s41586-022-05609-w (2022)

Dennis Schaefer-Babajew, Zijun Wang, Frauke Muecksch, Alice Cho, Maximilian Loewe, Melissa Cipolla, Raphael Raspe, Brianna Johnson, Marie Canis, Justin DaSilva, Victor Ramos, Martina Turroja, Katrina G. Millard, Fabian Schmidt, Leander Witte, Juan Dizon, Irina Shimelovich, Kai-Hui Yao, Thiago Y. Oliveira, Anna Gazumyan, Christian Gaebler, Paul D. Bieniasz, Theodora Hatziioannou, Marina Caskey & Michel C. Nussenzweig

Antibody feedback regulates immune memory after SARS-CoV-2 mRNA vaccination

Dennis Schaefer-Babajew[1,4], Zijun Wang[1,4], Frauke Muecksch[2,4], Alice Cho[1,4], Maximilian Loewe[1], Melissa Cipolla[1], Raphael Raspe[1], Brianna Johnson[1], Marie Canis[2], Justin DaSilva[2], Victor Ramos[1], Martina Turroja[1], Katrina G. Millard[1], Fabian Schmidt[2], Leander Witte[2], Juan Dizon[1], Irina Shimelovich[1], Kai-Hui Yao[1], Thiago Y. Oliveira[1], Anna Gazumyan[1, 3], Christian Gaebler[1], Paul D. Bieniasz[2, 3†], Theodora Hatziioannou[2†], Marina Caskey[1†] and Michel C. Nussenzweig[1, 3†]

[1]Laboratory of Molecular Immunology, The Rockefeller University, New York, NY 10065, USA

[2]Laboratory of Retrovirology, The Rockefeller University, New York, NY 10065, USA

[3]Howard Hughes Medical Institute, New York, NY, USA

[4]These authors contributed equally: Dennis Schaefer-Babajew, Zijun Wang, Frauke Muecksch, Alice Cho

†e-mail: pbieniasz@rockefeller.edu, thatziio@rockefeller.edu, mcaskey@rockefeller.edu or nussen@rockefeller.edu

Abstract/Summary

Feedback inhibition of humoral immunity by antibodies was first documented in 1909[1]. Subsequent work showed that, depending on the context, antibodies can enhance or inhibit immune responses[2,3]. However, little is known about how pre-existing antibodies influence the development of memory B cells. Here we examined the memory B cell response in individuals who received two high-affinity anti-SARS-CoV-2 monoclonal antibodies, and subsequently two doses of an mRNA vaccine[4-8]. We found that monoclonal antibody recipients produced antigen binding and neutralizing titers that were only fractionally lower than controls. In contrast, their memory B cells differed from controls in that they predominantly expressed low-affinity IgM antibodies that carried small numbers of somatic mutations and showed altered RBD target specificity consistent with epitope masking. Moreover, only 1 out of 77 anti-RBD memory antibodies tested neutralized the virus. The mechanism underlying these findings was examined in experiments in mice that showed that germinal centers (GCs) formed in the presence of the same antibodies were dominated by low-affinity B cells. Our results indicate that pre-existing high-affinity antibodies bias GC and memory B cell selection by two distinct mechanisms: (1) by lowering the activation threshold for B cells thereby permitting abundant lower-affinity clones to participate in the immune response, and (2) through direct masking of their cognate epitopes. This may in part explain the shifting target profile of memory antibodies elicited by booster vaccinations[9].

Main

To examine how passive administration of monoclonal antibodies (mAbs) might influence subsequent humoral responses to vaccination in humans, we studied a group of 18 healthy volunteers who received a single dose of the combination of two long-acting monoclonal antibodies to SARS-CoV-2 and subsequently received 2 doses of a SARS-CoV-2 mRNA vaccine (Fig. 1a). The 2 antibodies, C144-LS and C135-LS, bind Class 2 and 3 epitopes on the receptor binding domain (RBD) of the SARS-CoV-2 spike (S) protein with high affinity (K_D =18 nM and K_D = 6 nM, respectively) and neutralize the virus with IC50s of 2.55 and 2.98 ng/ml, respectively[5,8].

Between January 13 and March 3, 2021, 23 SARS-CoV-2-naïve individuals received C144-LS and C135-LS (n = 21) or placebo (n =2), in a first-in-human, phase 1 clinical trial at the Rockefeller University Hospital (NCT04700163). The antibodies were modified to extend their half-life by introducing the M428L and N343S mutations into their Fc domains[10] (LS). Individuals received a single dose of C144-LS and C135-LS IgG1 antibodies at a 1:1 ratio, starting with 100 mg of each subcutaneously (s.c.) in the lowest- and up to 15 mg/kg intravenously (i.v.) in the highest-dose group. Participants were followed longitudinally to assess the safety and tolerability of the infused mAbs and determine their pharmacokinetic properties.

Eighteen of the 21 phase 1 study participants who had received the monoclonal antibodies elected to receive SARS-CoV-2 mRNA vaccination and volunteered to enroll in a parallel observational study assessing their immune responses to SARS-CoV-2 vaccination (Supplementary Tables 1 and 2). The first and second vaccine doses were administered a median of 82 (range 42-110) and 103 (range 70-131) days after antibody administration (Supplementary Tables 1 and 2). At the time of vaccination, the plasma levels of C144-LS and C135-LS were between 5 and 100 μg/ml depending on the dosing group (Fig. 1b). The estimated half-lives of C144-LS and C135-LS were 69-99 days and 73-95 days, respectively.

The 18 vaccinated antibody recipients were compared to a cohort of 31 randomly selected mRNA vaccine recipients with no prior history of infection (Fig. 1a and Supplementary Tables 1, also see[9,11]). Both groups were sampled between 13-28 (median 19) and 15-91 (median 29) days after their first and second vaccine doses, respectively. The two cohorts were relatively matched for demographic characteristics and vaccine formulation (for details see Supplementary Tables 1 and 2), and none of the individuals included in the study seroconverted to nucleocapsid (N) at any time during observation period suggesting that they remained infection naïve.

Plasma antibody reactivity

Plasma IgM and IgG antibody binding activity against RBD were measured by ELISA using Wuhan-Hu-1 (WT) and mutant forms of RBD (R346S/E484K and N440K/E484K) that eliminate binding by C144 and C135 but not Class 1 or 4, or some affinity-matured Class 2 or 3 antibodies (Ext. Data Fig. 1a-f, also see[9,12]). When measured for WT RBD binding after one or two vaccine

doses, the IgM titers in mAb recipients were not significantly different from controls (Fig. 1c). In contrast, IgG anti-WT-RBD titers were significantly higher in mAb recipients than in controls after one vaccine dose but equalized following the second dose (Fig. 1d, $p<0.0001$ and $p=0.93$, respectively). The initial difference was attributed to the infused monoclonals because when the same samples were tested against either R346S/E484K or N440K/E484K mutant RBDs that interfere with C144 and C135 binding, plasma IgG antibody levels in the mAb recipient samples were slightly but not significantly lower than the controls (Fig. 1e). Conversely, the relative contribution of endogenous anti-RBD antibodies increased over time, as illustrated by a decrease in the correlation between the monoclonal antibody serum levels and plasma binding (Ext. Data Fig. 1g-h).

To determine whether the pre-existing antibodies to RBD interfered with humoral immunity to independent domains of the SARS-CoV-2 S protein, the same plasma samples were tested for binding to the N-terminal domain (NTD). IgG titers to NTD were similar in mAb recipients and controls (Fig. 1f). We conclude that high circulating levels of C144-LS and C135-LS do not interfere with IgM anti-RBD antibody responses and have only a small effect on IgG responses. Thus, the infused antibodies do not clear the vaccine antigen or measurably interfere with its overall ability to produce an immune response[13].

Neutralization

To assess plasma neutralizing activity, we used HIV-1 pseudotyped with WT or mutant S proteins that carry a furin-cleavage site mutation (R683G)[14]. As expected, based on the amount of C144-LS and C135-LS in circulation, neutralizing titers against WT were significantly higher in mAb recipients than in controls at both timepoints (Fig. 1g, $p<0.0001$). To determine the contribution of the endogenous neutralizing response to epitopes outside of the C144-LS and C135-LS target sites, we used viruses pseudotyped with S proteins containing the R346S/Q493K and R346S/N440K/E484K mutations that abolish the neutralizing activity of the 2 infused mAbs (Ext. Data Fig. 2a-d). Despite the initial dominance of Class 1-2 epitopes among neutralizing antibodies elicited by mRNA vaccination[6], the neutralizing titers of the control plasmas against the 2 mutant pseudoviruses were comparable to those against WT (Fig. 1h-i), suggesting that a significant proportion of circulating endogenous neutralizing antibodies are unaffected by the R346S/Q493K

and R346S/N440K/E484K mutations. After the first vaccine dose, mAb recipients showed significantly lower neutralizing titers against the mutant pseudoviruses than controls (2.7- and 3.5-fold for R346S/Q493K and R346S/N440K/E484K; Fig. 1h and i, p=0.0015 and p=0.014, respectively). Consistent with a recent report[13], neutralizing activity improved and was no longer significantly different from controls after the second vaccine dose (Fig. 1h and i). Similarly, we saw no discernible difference in plasma neutralization of the antigenically divergent BA.4/5 variant, which showed equal levels of immune evasion to the plasma antibodies in both groups (Ext. Data Fig. 2e). In conclusion, recipients of C144-LS and C135-LS had high initial levels of serum neutralizing activity due to the passively administered antibodies and they developed their own neutralizing antibodies that were not sensitive to RBD mutations in the C144/C135 target sites after mRNA vaccination.

Memory B cells

In addition to the plasma cells that produce circulating antibodies, vaccination also elicits memory B cells that contribute to protection upon re-exposure to the pathogen. These two cell types are selected by different mechanisms and, as a result, the antibodies they produce show differing levels of affinity to the immunogen[15-17]. Although the feedback effects of antibodies on humoral responses have been investigated extensively beginning in 1909[1,2], little is known about their effects on the development of memory B cells. To investigate the effects of passive mAb administration on B cell memory responses in humans, we used flow cytometry to enumerate and purify circulating memory B cells binding to phycoerythrin (PE) and Alexa-Fluor-647 (AF647) labeled RBDs (Ext. Data Fig. 3a-c)[5]. mRNA vaccination elicited robust RBD-specific memory B cell responses in mAb recipients that were approximately 4- and 3-fold higher than in controls after the first and second vaccine doses, respectively (Fig. 2a; $p<0.0001$ and $p<0.0001$, respectively). Thus, C144-LS and C135-LS administration increases the magnitude of the anti-RBD memory B cell response when compared to controls.

Human memory B cells represent a diverse pool of cells that can develop in germinal centers (GCs) or through an extrafollicular GC-independent pathway[18-20]. Memory B cells expressing class-switched and highly somatically mutated antibodies are primarily of germinal center origin[19,21]. IgM-expressing memory B cells, that express antibodies that carry only small

numbers of mutations typically develop by a germinal center independent pathway[22-25]. In control individuals, IgG-expressing RBD-specific memory cells comprised the majority of the memory B cell pool at both time points assayed. In line with the overall increase in anti-RBD memory cells, the absolute number of IgG-expressing cells was fractionally increased in mAb recipients (Ext. Data Fig. 3d). However, their relative contribution was significantly reduced at both time points, making up only 30 and 45% of the RBD-specific cells in mAb recipients after one and two doses, respectively (Fig. 2b; $p=0.0002$ and $p<0.0001$). Consistent with the relative decrease in IgG^+ memory B cells, more than half (57%) of the RBD-specific memory B cells from mAb recipients were cell surface IgM^+ after the first vaccine dose and this decreased only slightly to 49% after the second vaccine dose. In contrast, few such cells were found in the control group at that time (Fig. 2c and Ext. Data Fig. 3e; all $p<0.0001$). The skewed isotype ratio was correlated to the C144 serum concentration at the time of immunization (Ext. Data Fig. 3f-i). We conclude that pre-existing high-affinity anti-RBD antibodies alter the immune response to SARS-CoV-2 mRNA vaccination to favor the development of IgM-expressing memory B cells.

Memory B cell antibodies

To gain further insight into the effects of pre-existing antibodies on the human memory response to SARS-CoV-2 mRNA vaccination, we purified RBD-specific memory B cells from 5 representative mAb recipients after the second vaccine dose (Ext. Data Fig. 4a-b). A total of 353 and 856 paired antibody sequences from mAb recipients and previously characterized controls were examined, respectively (Fig. 2d, Ext. Data Fig. 4c-e and Supplementary Table 3, also see[11]). IgM transcripts accounted for 70-94% of sequences recovered from mAb recipients with an average of 9% belonging to expanded clones (Fig. 2d, upper panel and Fig. 2e). In contrast, IgG transcripts accounted for >90% of the immunoglobulin sequences isolated from controls (Fig. 2e and Ext. Data Fig. 4e). The relative IgM enrichment was more pronounced by the more sensitive PCR assay and may include cells that no longer express IgM on their surface. IgM memory cells originating from the extrafollicular non-GC pathway are generally less somatically mutated than IgG memory cells because they undergo fewer divisions[19,25]. Consistent with this idea, and the reversed ratio of IgM:IgG memory B cells in mAb recipients, the antibodies obtained from these individuals showed significantly fewer somatic mutations than controls (Fig. 2f, $p<0.0001$). However, when comparing IgM or IgG cells independently, the average mutational burden was

not significantly different between mAb recipients and controls (Fig. 2g, $p>0.99$ and $p=0.40$ for IgM and IgG, respectively). Thus, IgM- and IgG-expressing B cells in vaccinated individuals who had received C144-LS and C135-LS carry normal numbers of somatic mutations, but the relative ratio of the two memory cell types is reversed, which accounts for the overall lower level of mutation in their memory compartment. Finally, in contrast to controls there was no enrichment for VH3-53, VH1-69, VH1-46, and VH3-66 heavy chains, which often target Class 1 and 2 epitopes. Instead, there was relative enrichment for VH3-9, VH5-51, VH4-39, and VH1-8 genes (Ext. Data Fig. 4f). The limited number of cells sequenced precludes definitive conclusions about the precise clonotype distribution in this population, but the relative change in VH gene usage frequency implies that B cell recruitment into the memory compartment of mAb recipients is altered. In summary, the data suggest that pre-existing antibodies can alter the cellular and molecular composition of the RBD-specific MBC compartment that develops in response to mRNA vaccination.

To examine the binding and neutralizing activity of the memory antibodies elicited by mRNA vaccination in C144-LS and C135-LS recipients, we produced 178 representative monoclonals obtained from 5 individuals as IgGs and tested them for binding to the WT SARS-CoV-2 RBD by ELISA (Fig. 3a-c and Supplementary Table 4). In contrast to controls, where over 95% of the memory antibodies bound strongly to RBD, monoclonal antibodies isolated from volunteers that received C144-LS and C135-LS showed diverse levels of binding activity. Approximately one quarter (24%) of the antibodies displayed relatively poor binding with ELISA half-maximal effective concentrations (EC50s) that were only slightly above our limit of detection, and a little over one third (38%) showed no detectable binding above background (Fig. 3a-b). Accordingly, the median (EC50) of antibodies isolated from mAb recipients was significantly higher than in controls (Fig. 3b, $p<0.0001$). Notably, this difference remained significant when the monoclonals isolated from IgM and IgG memory cells were analyzed independently (Fig 3c, $p=0.0005$ and $p<0.0001$, respectively).

Memory antibodies obtained from C144-LS and C135-LS recipients that bound to WT SARS-CoV-2 RBD with EC50s <10 μg/ml were tested for neutralizing activity against viruses pseudotyped with WT spike. Whereas almost two thirds (63%) of the IgG and 17% of the IgM

antibodies isolated from controls showed measurable neutralizing activity, only 1 out of 45 IgG- and none of the 32 IgM-derived antibodies obtained from C144-LS and C135-LS recipients neutralized SARS-CoV-2 (Fig. 3d-e). Thus, the antibodies isolated from the RBD-specific memory B cell compartment of vaccinated mAb recipients show significantly less neutralizing activity than controls. In circulation, IgM antibodies are pentamers which, in addition to their superior ability to fix complement, show increased apparent affinities. To test whether the binding and neutralizing properties of IgM antibodies would be improved when expressed as pentamers, we re-expressed 17 IgM memory antibodies (15 from mAb recipients and 2 from controls) as pentameric IgMs. Although the pentamers obtained from mAb recipients showed significantly improved binding to RBD by ELISA (Ext. Data Fig. 5a and Supplementary Table 4; $p=0.0004$), they remained unable to neutralize (Ext. Data Fig. 5b and Supplementary Table 4). In contrast, both control IgM antibodies showed improved neutralizing potency when expressed as pentamers (Ext. Data Fig. 5b).

To examine the affinity of the antibodies, we performed biolayer interferometry experiments (BLI) in which monoclonal antibodies were immobilized on the biosensor chip and exposed to WT RBD monomers[12] (Fig. 3f and g). In contrast to controls, where 96% of the antibodies tested displayed measurable affinities, only two thirds (67%) of the antibodies derived from mAb recipients did so (Fig. 3g, i and k, $p<0.0001$). When all antibodies were considered together, the median affinity (Kd) differed by nearly one order of magnitude between mAb recipients and controls (Fig. 3k, $p<0.0001$). Moreover, this difference remained significant when IgM and IgG monoclonals were considered independently (Fig 3l, $p =0.0058$ and $p<0.0001$, respectively), indicating that the lower affinities observed in the memory compartment of mAb recipients cannot solely be explained by the preponderance of IgM.

C144-LS and C135-LS have the potential to form immune complexes with the vaccine antigen *in vivo* and present it as a multimer that could increase the apparent affinity of a B cell for the multimerized antigen by avidity effects. To determine whether memory cell-derived antibodies from mAb recipients with no apparent affinity to monomeric antigen would show binding under higher valency conditions, we exposed the immobilized monoclonals to biotin-streptavidin tetramerized trimers of S (Fig. 3f, h and j). Of the 25 antibodies with no apparent monomeric

binding tested, 23 (92%) bound to multimerized S (Fig. 3h and j). We conclude that most of the anti-RBD antibodies isolated from mAb recipients that failed to show detectable binding to RBD monomers bind to multimerized antigen. Thus, the absence of binding to monomeric antigen is a consequence of the relatively low affinity of the memory antibodies derived from mAb recipients and not due to altered specificity.

To examine the epitopes targeted by the vaccine-elicited anti-RBD antibodies produced by memory B cells of C144-LS and C135-LS recipients, we performed BLI experiments in which a pre-formed antibody-RBD complex composed of one of 4 structurally characterized antibodies[8,26,27] was exposed to a second monoclonal targeting an unknown epitope (Fig. 3m and Ext. Data Fig. 6). 49% of the anti-RBD memory antibodies obtained from vaccinated controls target Class 1, 2 or 3 epitopes or combinations thereof (Fig. 3n, Ext. Data Fig. 6a-f, and [9,11]). In contrast, only 20% of the memory antibodies obtained from mAb recipients targeted Class 1 or 2 epitopes, and none were Class 3-specific. Instead, we found that 78% of these antibodies targeted either Class 4-containing epitopes or epitopes that could not be classified by our method (Fig. 3n and Ext. Data Fig. 6a-f). Thus, there was a significant shift in the distribution of epitopes targeted by memory antibodies isolated from mAb recipients compared to controls (Fig. 3n, p=0.0089). In conclusion, C144-LS and C135-LS alter the development of memory B cells expressing anti-RBD antibodies and their epitope target preference.

Germinal center (GC) B cell responses

To examine the mechanism by which pre-existing antibodies alter memory B cell selection, we immunized wild-type C57BL/6 mice pre-infused with C135 and C144 or an irrelevant anti-HIV mAb cocktail with recombinant SARS-CoV-2 RBD (Fig. 4a). Mice pre-treated with control anti-HIV antibodies developed GC responses in which an average of 27% of the B cells bound to RBD (Fig. 4b-c and Ext. Data Fig. 7a-d). Although GC size was not altered in mice that received C135 and C144 (Fig. 4b and Ext. Data Fig. 7c), the fraction of RBD-binding cells was significantly reduced (Fig. 4c and Ext. Data Fig. 7b, d; p=0.041).

To examine the molecular nature of the memory antibodies produced in the presence of pre-existing high-affinity antibodies, we cloned and produced antibodies from GC B cells. A total of

351 and 352 antibodies were obtained from the anti-RBD- and anti-HIV-treated control groups, respectively (Supplementary Table 5). B cells isolated from both groups showed similar levels of somatic mutation (Ext. Data Fig. 7e), and clonal expansion (Fig. 4d and Ext. Data Fig. 7f). However, in the C135 and C144 recipients clonally expanded and unique B cells were dominated by cells that failed to bind RBD by flow cytometry (Fig. 4d-e, p=0.046 and p=0.026, respectively).

106 monoclonal antibodies were expressed as Fabs (Supplementary Table 6) and tested for binding to SARS-CoV-2 RBD by biolayer interferometry (BLI, Fig. 4f). Under monomeric binding conditions 46% (22/47) of the Fabs derived from control mice bound to RBD (Fig. 4g). In contrast, only 21% (8/46) of the GC B cell antibodies from mice pre-treated with C135 and C144 showed measurable but demonstrably lower affinity under these conditions (Fig. 4g-i, p=0.0036 and Ext. Data Fig. 7g). Thus, our mouse immunization experiments show that pre-existing high affinity antibodies lower the affinity threshold for B cell participation in immune responses, and thereby provide a mechanistic explanation for the observation that the memory compartment in humans infused with C135 and C144 is dominated by low-affinity B cells.

Discussion

Our experiments show that pre-existing antibodies alter the development of memory B cells in response to SARS-CoV-2 mRNA vaccination in humans. Consistent with a recent report, C144-LS and C-135-LS did not significantly interfere with the development of circulating antibodies that bind to epitopes outside of the target sites of the two monoclonal antibodies[13]. And while we found that endogenous neutralizing responses were reduced in mAb recipients after one dose, this difference was no longer significant after two doses of mRNA vaccination. In contrast, anti-RBD-specific memory B cell development was profoundly altered. Specifically, the affinity threshold for entry into the memory and GC B cell compartment in humans and mice was lowered, and there was a change in the epitopes targeted in the presence of pre-existing antibodies.

Memory cells expressing IgG antibodies specific to Class 1, 2 or 3 epitopes normally dominate the anti-RBD response after 2 doses of mRNA vaccination[4-8]. In contrast, we found that mAb recipients develop increased numbers of IgM anti-RBD memory cells that express antibodies with altered epitope specificity consistent with epitope masking. This may also explain the shift in

memory B cell specificity away from Class 1 and 2 after the 3rd dose of the SARS-CoV-2 mRNA vaccines that increases the breadth of the neutralizing response[9].

Beginning with experiments on anti-Diptheria toxin antibodies in the early part of the 20th century, extensive work in experimental animals showed that passive transfer of polyclonal immune serum or monoclonal antibodies can alter subsequent humoral immune responses in an epitope-specific manner[1,2]. More recently, epitope masking by pre-existing antibodies was shown to interfere with the epitope-specific plasmablast response to Malaria vaccination[28,29]. In Malaria vaccine trials a 3rd vaccine dose produced a smaller fraction of high-affinity antibody producing plasmablasts than the 2nd, and this was attributed to epitope masking. The masking effect of pre-existing high-affinity antibodies was confirmed in transgenic mice that showed high-affinity antibodies block B cell entry into GCs in an epitope-specific manner[29-31]. However, these results were obtained in the context of a restricted transgenic B cell repertoire and the effect of pre-existing antibodies on the development of memory B cells in polyclonal responses was not examined[29] . The results of our clinical trial and mouse experiments agree with the observation that pre-existing antibodies block the development of epitope-specific B cells[32,33]. Our experiments extend prior observations because we also examined the specificity and antigen binding affinity of the antibodies produced by B cells that do respond to antigen in the presence of pre-existing antibody. An unexpected finding was that pre-existing high-affinity antibodies lower the affinity threshold for B cell participation in the immune response. As a result, the anti-SARS-CoV2 antibodies expressed by memory B cells developing in humans that received monoclonal antibody infusions prior to vaccination are dominantly of low affinity. In contrast, low-affinity polyclonal antibodies emerging after a vaccine prime may enhance vaccine booster responses by mechanisms that remain to be fully elucidated[2,3,31].

Memory B cells can develop by 2 different pathways[18,19]. Class-switched memory B cells that carry relatively higher-affinity antibodies with large numbers of somatic mutations develop in germinal centers (GCs). In contrast, IgM-expressing memory B cells that carry lower-affinity antibodies and only small numbers of mutations develop by a GC-independent pathway[18,20]. Our human data suggest that the passive transfer of C144-LS and C135-LS may favor the GC-independent pathway by creating immune complexes (reviewed in [34]). Immune complexes trap

and sequester antigen in lymphoid organs and thereby increase local antigen concentration. In addition, they contain multiple copies of the antigen in a form that increases apparent affinity by avidity effects, thereby enabling the recruitment of B cells with very low-affinity receptors into the immune response[34]. Together, the increased antigen concentration and avidity effects combine to reduce selection stringency and help explain the increase in low-affinity RBD-binding B cells found in human mAb recipients, as this allows for the activation of greater numbers of abundant lower-affinity clones which would otherwise fail to be recruited to the immune response. Thus, the combination of epitope masking and lowered affinity thresholds diversify the ensuing B cell responses.

In conclusion, the composition of germinal centers and the development of memory in response to vaccination are influenced by pre-existing antibodies that can alter the antibody target profile, affinity, and isotype of the responding cells. Diversification of the antibody response by this mechanism may help increase the breadth of vaccines like the SARS-CoV-2 vaccine but interfere with the development of breadth and potency in others, like HIV-1 or influenza, by diverting immunity away from broadly neutralizing to strain-specific epitopes and by allowing increasing numbers of low-affinity precursors expressing off-target antibodies to participate in the immune response.

References:

1 Smith, T. ACTIVE IMMUNITY PRODUCED BY SO CALLED BALANCED OR NEUTRAL MIXTURES OF DIPHTHERIA TOXIN AND ANTITOXIN. *J Exp Medicine* **11**, 241-256, doi:10.1084/jem.11.2.241 PMID - 19867246 (1909).

2 Heyman, B. Regulation of Antibody Responses via Antibodies, Complement, and Fc Receptors. *Annu Rev Immunol* **18**, 709-737, doi:10.1146/annurev.immunol.18.1.709 PMID - 10837073 (2000).

3 Bournazos, S. & Ravetch, J. V. Fcgamma Receptor Function and the Design of Vaccination Strategies. *Immunity* **47**, 224-233, doi:10.1016/j.immuni.2017.07.009 (2017).

4 Brouwer, P. J. M. *et al.* Potent neutralizing antibodies from COVID-19 patients define multiple targets of vulnerability. *Science* **369**, 643-650, doi:10.1126/science.abc5902 PMID - 32540902 (2020).

5 Robbiani, D. F. *et al.* Convergent antibody responses to SARS-CoV-2 in convalescent individuals. *Nature* **584**, 437-442, doi:10.1038/s41586-020-2456-9 (2020).

6 Wang, Z. *et al.* mRNA vaccine-elicited antibodies to SARS-CoV-2 and circulating variants. *Nature* **592**, 616-622, doi:10.1038/s41586-021-03324-6 PMID - 33567448 (2021).

7 Yuan, M. *et al.* Structural and functional ramifications of antigenic drift in recent SARS-CoV-2 variants. *Sci New York N Y* **373**, eabh1139, doi:10.1126/science.abh1139 PMID - 34016740 (2021).

8 Barnes, C. O. *et al.* SARS-CoV-2 neutralizing antibody structures inform therapeutic strategies. *Nature* **588**, 682-687, doi:10.1038/s41586-020-2852-1 (2020).

9 Muecksch, F. *et al.* Increased Memory B Cell Potency and Breadth After a SARS-CoV-2 mRNA Boost. *Nature*, 1-6, doi:10.1038/s41586-022-04778-y PMID - 35447027 (2022).

10 Zalevsky, J. *et al.* Enhanced antibody half-life improves in vivo activity. *Nature biotechnology* **28**, 157 - 159, doi:10.1038/nbt.1601 PMID - 20081867 (2010).

11 Cho, A. *et al.* Anti-SARS-CoV-2 receptor-binding domain antibody evolution after mRNA vaccination. *Nature* **600**, 517-522, doi:10.1038/s41586-021-04060-7 (2021).

12 Wang, Z. *et al.* Naturally enhanced neutralizing breadth against SARS-CoV-2 one year after infection. *Nature* **595**, 426-431, doi:10.1038/s41586-021-03696-9 (2021).

13 Benschop, R. J. *et al.* The anti-SARS-CoV-2 monoclonal antibody bamlanivimab minimally affects the endogenous immune response to COVID-19 vaccination. *Sci Transl Med* **14**, eabn3041, doi:10.1126/scitranslmed.abn3041 (2022).

14 Schmidt, F. *et al.* Measuring SARS-CoV-2 neutralizing antibody activity using pseudotyped and chimeric viruses. *J Exp Med* **217**, e20201181, doi:10.1084/jem.20201181 PMID - 32692348 (2020).

15 Viant, C. *et al.* Antibody Affinity Shapes the Choice between Memory and Germinal Center B Cell Fates. *Cell* **183**, 1298-1311 e1211, doi:10.1016/j.cell.2020.09.063 (2020).

16 Ise, W. *et al.* T Follicular Helper Cell-Germinal Center B Cell Interaction Strength Regulates Entry into Plasma Cell or Recycling Germinal Center Cell Fate. *Immunity* **48**, 702-715 e704, doi:10.1016/j.immuni.2018.03.027 (2018).

17 Phan, T. G. *et al.* High affinity germinal center B cells are actively selected into the plasma cell compartment. *J Exp Medicine* **203**, 2419-2424, doi:10.1084/jem.20061254 PMID - 17030950 (2006).

18 Kurosaki, T., Kometani, K. & Ise, W. Memory B cells. *Nat Rev Immunol* **15**, 149-159, doi:10.1038/nri3802 PMID - 25677494 (2015).

19 Victora, G. D. & Nussenzweig, M. C. Germinal Centers. *Annu Rev Immunol* **40**, 413-442, doi:10.1146/annurev-immunol-120419-022408 (2022).

20 Weisel, F. & Shlomchik, M. Memory B Cells of Mice and Humans. *Annu Rev Immunol* **35**, 1-30, doi:10.1146/annurev-immunol-041015-055531 PMID - 28142324 (2015).

21 Klein, U., Rajewsky, K. & Küppers, R. Human Immunoglobulin (Ig)M+IgD+ Peripheral Blood B Cells Expressing the CD27 Cell Surface Antigen Carry Somatically Mutated Variable Region Genes: CD27 as a General Marker for Somatically Mutated (Memory) B Cells. *J Exp Medicine* **188**, 1679-1689, doi:10.1084/jem.188.9.1679 PMID - 9802980 (1998).

22 Klein, U., Küppers, R. & Rajewsky, K. Evidence for a Large Compartment of IgM-Expressing Memory B Cells in Humans. *Blood* **89**, 1288-1298, doi:10.1182/blood.v89.4.1288 (1997).

23 Taylor, J. J., Pape, K. A. & Jenkins, M. K. A germinal center–independent pathway generates unswitched memory B cells early in the primary response. *J Exp Medicine* **209**, 597-606, doi:10.1084/jem.20111696 PMID - 22370719 (2012).

24 Viant, C. *et al.* Germinal center–dependent and –independent memory B cells produced throughout the immune response. *J Exp Med* **218**, e20202489, doi:10.1084/jem.20202489 PMID - 34106207 (2021).

25 Weisel, Florian J., Zuccarino-Catania, Griselda V., Chikina, M. & Shlomchik, Mark J. A Temporal Switch in the Germinal Center Determines Differential Output of Memory B and Plasma Cells. *Immunity* **44**, 116-130, doi:10.1016/j.immuni.2015.12.004 PMID - 26795247 (2016).

26 Barnes, C. O. *et al.* Structures of Human Antibodies Bound to SARS-CoV-2 Spike Reveal Common Epitopes and Recurrent Features of Antibodies. *Cell* **182**, 828-842 e816, doi:10.1016/j.cell.2020.06.025 (2020).

27 Jette, C. A. *et al.* Broad cross-reactivity across sarbecoviruses exhibited by a subset of COVID-19 donor-derived neutralizing antibodies. *Cell Reports* **36**, 109760-109760, doi:10.1016/j.celrep.2021.109760 PMID - 34534459 (2021).

28 Kurtovic, L., Boyle, M. J. & Beeson, J. G. Epitope masking may limit antibody boosting to malaria vaccines. *Immunol Cell Biol* **99**, 126-129, doi:10.1111/imcb.12415 PMID - 33152796 (2021).

29 McNamara, H. A. *et al.* Antibody Feedback Limits the Expansion of B Cell Responses to Malaria Vaccination but Drives Diversification of the Humoral Response. *Cell Host Microbe* **28**, 572-585.e577, doi:10.1016/j.chom.2020.07.001 PMID - 32697938 (2020).

30 Pape, K. A., Taylor, J. J., Maul, R. W., Gearhart, P. J. & Jenkins, M. K. Different B cell populations mediate early and late memory during an endogenous immune response. *Science* **331**, 1203-1207, doi:10.1126/science.1201730 (2011).

31 Tas, J. M. J. *et al.* Antibodies from primary humoral responses modulate recruitment of naive B cells during secondary responses. *Immunity* **55**, 1856-1871 e1856, doi:10.1016/j.immuni.2022.07.020 (2022).

32 Meyer-Hermann, M. Injection of Antibodies against Immunodominant Epitopes Tunes Germinal Centers to Generate Broadly Neutralizing Antibodies. *Cell Reports* **29**, 1066-1073.e1065, doi:10.1016/j.celrep.2019.09.058 PMID - 31665624 (2019).

33 Zarnitsyna, V. I., Lavine, J., Ellebedy, A., Ahmed, R. & Antia, R. Multi-epitope Models Explain How Pre-existing Antibodies Affect the Generation of Broadly Protective Responses to Influenza. *PLoS Pathog* **12**, e1005692, doi:10.1371/journal.ppat.1005692 (2016).

34 Heesters, B. A., Myers, R. C. & Carroll, M. C. Follicular dendritic cells: dynamic antigen libraries. *Nat Rev Immunol* **14**, 495-504, doi:10.1038/nri3689 PMID - 24948364 (2014).

35 Meffre, E. *et al.* Surrogate light chain expressing human peripheral B cells produce self-reactive antibodies. *The Journal of experimental medicine* **199**, 145-150, doi:10.1084/jem.20031550 (2004).

Main figures

Fig. 1: Study design and plasma antibody activity.

a, Schematic overview of the study design with markers (w) denoting weeks relative to the time of the first vaccine dose. **b,** Serum levels of C135-LS (upper panel, in blue) and C144-LS (lower panel, in red) over time are shown. The thick colored dashed lines indicate the median serum concentrations among monoclonal antibody (mAb) recipients (n=18), while the thin dotted black lines represent individual participants. The two solid vertical lines indicate the median and the grey shaded areas the range of time from mAb administration. **c-f,** Half-maximal plasma binding titers (BT50) to RBD after one (vax1) and two doses (vax2) of mRNA vaccination for mAb recipients (n=18, in green) and controls (n=26, in blue). Each dot represents one individual. Dashed horizontal lines represent the median binding activity of healthy pre-pandemic plasma samples, which served as negative controls. **c,d,** IgM (**c**) and IgG (**d**) binding titers to WT RBD. **e,** IgG binding to R346S/E484K (left panel) and N440K/E484K RBDs (also Ext. Data Fig. 1). **f,** IgG binding to the NTD. **g-i,** Plasma half-maximal neutralizing titers (NT50s) for mAb recipients (n=18, in green) and controls (n=26, in blue) against HIV-1 pseudotyped with **g,** SARS-CoV-2 WT S. **h,** R346S/Q493K mutant S. **i**, R346S/N440K/E484K mutant S (also Ext. Data Fig. 2). The S protein in the pseudoviruses in **g-i** contained an R683G substitution. Red horizontal bars in **c-i** and red numbers in **g-i** represent median values. Statistical significance in **c-i** was determined using the two-tailed Mann-Whitney test comparing differences between mAb recipients and controls for each time point independently. All experiments were performed at least in duplicate.

Fig. 2: Anti-SARS-CoV-2 RBD memory B cells from vaccinated mAb recipients.

a-c, Flow-cytometric enumeration and surface immunoglobulin expression of SARS-CoV-2 RBD-specific memory B cells after vax1 and vax2 isolated from mAb recipients (green, n=18) and controls[9,11] (blue, n=26 for vax1 and n=31 for vax2 in panel **a**, and n=10 in panels **b,c**). Each dot represents one individual, red horizontal bars (and numbers in panel **a**) depict median values. **a,** Number of WT RBD-specific memory B cells per 10 million $CD20^+$ B cells (also Ext. Data Fig 3a and b). **b,c,** Percentage of cells among WT RBD-binding $CD20^+$ B cells that express cell surface IgG (**b**) or IgM (**c**). **d,** Pie charts show distribution of antibody sequences derived from cells isolated from 5 vaccinated mAb recipients after vax2 (also Ext. Data Fig. 3d and e). Upper panel shows IgM, lower panel IgG. Numbers in the inner circles indicate the number of sequences analyzed for the respective individual. Green colored slices indicate clonally expanded cells (same IGHV and IGLV genes, with highly similar CDR3s) within an individual. Pie slice size is proportional to the number of clonally related sequences, with the fraction of clonally expanded sequences summarized in % (black outline). White pie areas indicate proportion of sequences isolated only once. **e,**

Fraction of cells harboring IgG (black) vs. IgM (white) transcripts per individual (also Ext. Data Fig. 3f and [9,11]). **f,g,** Somatic hypermutation (SHM) shown as combined heavy- and light-chain variable region nucleotide substitutions plus one (IGVH+IGVL+1), with each dot representing one sequence from mAb recipients (green) or controls (blue). Ring plots below show fraction of sequences with no (IGVH+IGVL+1 = 1) vs. any (IGVH+IGVL+1 > 1) SHM, and encircled numbers indicate the number of sequences analyzed, for all cells irrespective of isotype (**f**), and IgM and IgG analyzed independently (**g**). Red horizontal bars and numbers in **f** and **g** indicate mean values. Statistical significance was determined using the two-tailed Mann-Whitney test for **a-c** and **f**, the Kruskal-Wallis test with subsequent Dunn's correction for multiple comparisons for **g**, and the two-sided Fisher's exact test to compare fractions in **f** and **g**.

Fig. 3: Anti-SARS-CoV-2 RBD memory antibodies from vaccinated mAb recipients.

a-c, Monoclonal antibody binding to WT RBD. **a,** Graph shows ELISA binding of monoclonal memory antibodies derived from mAb recipients. Each curve represents one antibody. Green curves show EC50s <10 μg/ml, grey dashed lines EC50s >10 μg/ml, solid black lines are antibodies that were below or equal to a negative control anti-HIV1 antibody 3BNC117 (thick, white-dashed line). C144 (thick, red-dashed line) is a positive control. **b,** Summary of EC50s derived from (**a**) mAb recipients (green), and controls (blue) for all antibodies irrespective of isotype. **c,** as in (**b**) but IgM and IgG analyzed independently. Grey shaded area between horizontal dotted lines indicates antibodies with EC50s >10 μg/ml (poor binding) and non-binding antibodies arbitrarily grouped at 10 and 20 μg/ml, respectively. Ring plots summarize the fraction of all antibodies tested for the respective groups (encircled number). **d,** Plots show IC50s for all monoclonal antibodies isolated from vaccinated mAb recipients (green) or controls (blue). Ring plots illustrate the fraction of non-neutralizing (IC50 > 1000 ng/ml) antibodies (black slices) among all antibodies tested for the respective group (encircled number). **e,** as in (**d**) but IgM and IgG antibodies analyzed independently. **f-l,** Monoclonal antibody binding to monomeric and multimerized antigen by BLI. **f,** Schematic of monomeric binding measurements where IgG is immobilized on the biosensor chip and subsequently exposed to monomeric RBD (upper panel), and multimeric binding using 6P-stabilized WT SARS-CoV-2 S protein trimers that had been tetramerized using streptavidin (lower panel). **g,** Graphs show BLI traces obtained under monovalent conditions as illustrated in (**f**, upper panel). Each curve represents one antibody. Colored solid lines denote binding above background represented by polyreactive antibody ED38[35] (dotted black line) and anti-HIV-1 antibody 3BNC117 (dashed black line). Grey lines show non-binding antibodies. C144 (thick, red-dashed line) is a positive control. Colored and grey numbers in upper left of each panel indicate the number of binding and non-binding antibodies, respectively. **h**, As in (**g**) for antibodies that showed no measurable binding in (**g**) and were subsequently tested for binding under polyvalent conditions as illustrated in (**f**, lower panel). **i,** Bar charts show the percentage of binding

antibodies under monovalent conditions for all antibodies and by isotype. Values below bars indicate the number of antibodies tested. **j** as in (**i**) for antibodies shown in (**h**). **k,** Graphs show affinity constants (K_d) derived under monomeric binding conditions (**g)** for mAb recipients (green) and controls (blue) irrespective of isotype. Ring plots illustrate the fraction of antibodies tested for the respective group (encircled number) that measurably bound to monomeric RBD ("binding", in white) and those for which a K_d value could not be established ("no K_d", black). **l**, as in (**k**) analyzed independently for IgM and IgG. **m**, Schematic representation of BLI competition experiment: (1) capture antibody of known epitope-specificity (class-reference antibody) is bound to the biosensor chip, (2) exposed to antigen, and (3) the antibody of interested is added to the chip. **n**, Pie charts show the distribution of epitopes targeted. The number in the center is the number of antibodies tested. Slices colored in shades of red and blue represent Class 1, 2 and 3 or combined epitopes, shades of grey represent Class 4-containing epitopes or epitopes that could not be classified. For panels **b-e**, **k** and **l** red horizontal bars and numbers represent median values (N/D, not determined). Statistical significance was determined using the two-tailed Mann-Whitney test for **b**, **d** and **k**, the Kruskal-Wallis test with subsequent Dunn's correction for multiple comparisons for **c**, **e** and **l,**, the two-sided Fisher's exact test for **d**, **e**, **k** and **l**, and the two-sided Chi-squared contingency statistic for panels **b**, **c** and **n**.

Fig. 4: Germinal center (GC) responses in mAb pre-treated mice.

a, Schematic of the experimental setup. Pooled popliteal lymph nodes (dLN) were analyzed by flow-cytometry (also Ext. Data Fig. 7 and methods). In panels **b-i**, control mice pre-treated with irrelevant anti-HIV mAbs (3BNC117 and 10-1074, n=6) are in blue, and mice that received the combination of C135 and C144 (n=6) are in green. **b-c,** Enumeration of germinal center (GC) B cells (CD38- Fas+ GL7+) as a fraction of all B220+ B cells (**b**) and RBD-binding cells as a fraction of GC B cells (**c**). **d-e**, Antibody sequences from single GC B cells. **d**, Pie charts show distribution of antibody sequences. Encircled numbers indicate the number of sequences analyzed per animal. Solid pie slices indicate clonally expanded sequences, with slices colored in shades of blue (controls) or green (anti-RBD mAb group) indicating binding clones (as in Ext. Data Fig. 7b and Supplementary Table 5). Grey slices denote non-binding clones. Sequences appearing only once are stippled (binding) or white (non-binding). **e**, Relative contribution of binding clones and singlets in (**d**). **f-i**, Binding of monoclonal GC B cell-derived Fabs to monomeric RBD by biolayer interferometry (BLI). **f**, illustrates BLI setup. **g-h**, Graphs show traces of Fabs derived from controls (**g**) and anti-RBD treated mice (**h**). Each curve represents one Fab. Colored solid lines denote binding above background represented by polyreactive antibody ED38[35] (dashed black line) and negative control antibody mGO53 (dotted black line). Grey lines show non-binding antibodies. C144 (thick, red-dashed line) is a positive control. Colored and grey numbers in the upper left of each

panel indicate the number of binding and non-binding antibodies, respectively. **i**, Bar charts show the percentage of binding Fabs, with the total number of Fabs tested from the control (n=47) and anti-RBD mAb group (n=46) denoted below. In panels **b**, **c** and **e,** colored dots represent individual mice and red horizontal lines in indicate median values. Statistical significance was determined using the two-tailed Mann-Whitney test for **b**, **c** and **e**, and two-sided Fisher's exact test for **i**.

Methods

Study participants.

Participants in the "monoclonal antibody recipient" group were healthy SARS-CoV-2-naïve volunteers who were enrolled in a first-in-human phase 1 study at the Rockefeller University Hospital in New York and received single doses of two anti-SARS-CoV-2 RBD monoclonal antibodies (mAbs), C144-LS and C135-LS, between January 13 and March 3, 2021 (NCT04700163). The phase 1 clinical trial had a dose escalation design and evaluated the safety and tolerability, and pharmacokinetics of the two mAbs. The mAb cocktail (1:1 ratio of C144-LS and C135-LS) was administered to 21 out of the 23 enrolled individuals (n=2 receiving placebo), allowing for multiple interim safety analyses. The mAbs were administered at 100 or 200 mg each, subcutaneously, or at 1, 5 or 15 mg/kg each, intravenously (see Supplementary Table 2). Eligible participants for the phase 1 study were healthy adults with no history of SARS-CoV-2 infection or vaccination, or prior receipt of any SARS-CoV-2 therapeutics, including other monoclonal antibodies or convalescent plasma. Further details on inclusion and exclusion criteria, study design and endpoints of the phase 1 study can be found on clinicaltrials.gov (NCT04700163). Of the 21 individuals who received the mAbs in the phase 1 study, 18 co-enrolled in a parallel observational study to assess their immune responses to subsequent SARS-CoV-2 mRNA vaccination. One individual chose to receive the Janssen (Ad26.COV2.S) vaccine, and another individual (a placebo recipient) displayed Nucleocapsid (N) titer changes prior to enrollment in the observational study that were compatible with a recent SARS-CoV-2 infection, making them ineligible for inclusion in this study. The remaining phase 1 study participant chose not to enroll in the parallel study of immune responses. The 18 mAb-recipients included in this observational study received either the Moderna (*Spikevax,* mRNA-1273) or Pfizer-BioNTech (*Comirnaty,* BNT162b2) mRNA vaccines against the wildtype (Wuhan-Hu-1) strain of the severe acute respiratory syndrome coronavirus 2 (SARS-CoV-2). Participants in the "vaccinated control" group were healthy SARS-CoV-2-naïve volunteers who had received two doses of one of the two currently approved SARS-CoV-2 mRNA vaccines, Moderna (*Spikevax,* mRNA-1273) or Pfizer-BioNTech (*Comirnaty,* BNT162b2) mRNA vaccines. These control individuals had been recruited to the Rockefeller University Hospital for serial blood donations to longitudinally assess their immune responses to SARS-CoV-2 mRNA vaccination[9,11]. We previously reported the findings obtained from this group and refer to Cho et

al.[11] and Muecksch et al.[9] for further details on participant recruitment, inclusion and exclusion criteria, and demographic characteristics (also see Supplementary Tables 1 and 2). At each sample collection visit, participants of either group presented to the Rockefeller University Hospital for blood sample collection and were asked to provide details of their vaccination regimen, possible side effects, comorbidities, and possible COVID-19 history. Vaccinations were administered outside of the study, at the discretion of the individual and their health care provider consistent with existing guidelines and, as such, not influenced by their participation in our study. Baseline and longitudinal plasma samples were tested for binding activity toward the nucleocapsid protein (N; Sino Biological, 40588-V08B) of SARS-CoV-2. Absence of seroconversion toward N during the study interval was used to exclude SARS-CoV-2 infection, in addition to participants' reported history. Clinical data collection and management were carried out using the software iRIS by iMedRIS (v. 11.02). All participants provided written informed consent before participation in the study, which was conducted in accordance with Good Clinical Practice. The study was performed in compliance with all relevant ethical regulations, and the clinical protocols (CGA-1015 and DRO-1006) for studies with human participants were approved by the Institutional Review Board of the Rockefeller University. For detailed participant characteristics see Supplementary Tables 1 and 2, and [9,11]

Blood samples processing and storage.

Peripheral Blood Mononuclear Cells (PBMCs) obtained from samples collected at Rockefeller University were purified as previously reported by gradient centrifugation and stored in liquid nitrogen in the presence of Fetal Calf Serum (FCS) and Dimethylsulfoxide (DMSO)[5]. Heparinized plasma and serum samples were aliquoted and stored at -20°C or less. Prior to experiments, aliquots of plasma samples were heat-inactivated (56°C for 1 hour) and then stored at 4°C.

Pharmacokinetics of C144-LS and C135-LS

To evaluate the pharmacokinetic (PK) properties of the passively administered antibodies, C144-LS and C135-LS, their serum antibody levels were measured on the day of antibody administration (day 0) at 1, 3,6, 9 and 12 hours after infusion, and on days 1, 3, 7, 14, 21, 28, 56, 84, 126, 168, 252, and 336. C144-LS and C135-LS levels in serum were measured by mass-spectrometry (MS/MS). Briefly, analytes were isolated from serum samples through

immunocapture using streptavidin beads and biotinylated RBD protein. The isolated proteins were denatured with dithiothreitol, alkylated with iodoacetamide, and digested with trypsin. The final extract was analyzed via high-performance liquid chromatography (HPLC) with column-switching and MS/MS detection using positive ion electrospray. A linear, 1/concentration^2 weighted, least-squares regression algorithm was used for quantification. Noncompartmental analysis (NCA) was used to estimate PK parameters from measured serum levels of C144-LS and C135-LS. Phoenix WinNonlin® (v8.2) was used for the NCA. Actual sample time post administration of each mAb was used for the estimation of serum PK parameters instead of nominal time. Half-life estimates were similar between administration routes for both C144-LS and C135-LS, indicating a half-life of 2-3 months for both mAbs by either administration route (C144-LS: 68.9 to 99.3 days for s.c. groups and 86.9 to 92.3 days for i.v. groups; C135-LS: 72.7 to 77.9 days for s.c. groups and 70.5 to 94.7 days for i.v. groups). Visualization of the PK data was performed in GraphPad Prism, using the three-phase decay model.

Mouse immunizations

C57BL/6J mice were purchased from Jackson. All mice used were females aged 6-12 weeks at the start of the experiments. Mice were housed at a temperature of 72 °F and humidity of 30–70% in a 12-h light/dark cycle with ad libitum access to food and water. Footpad immunizations were performed using 25 µL of 1x PBS containing 5 µg of recombinant RBD and 8.5 µl of 2% Alhydrogel (Invivogen 21645-51-2). 3BNC117/10-1074 and C135/C144 antibody cocktails were prepared with 100 ug of each antibody and delivered in 1x PBS via i.v. injection. All animal procedures and experiments were performed without blinding or randomization, and according to protocols approved by the Rockefeller University Institutional Animal Care and Use Committee (IACUC).

ELISAs

Enzyme-Linked Immunosorbent Assays (ELISAs)[36,37] to evaluate antibodies binding to SARS-CoV-2 Wuhan-Hu-1 RBD, NTD or S were performed by coating of high-binding 96-half-well plates (Corning 3690) with 50 µl per well of a 1 µg/ml protein solution in Phosphate-buffered Saline (PBS) overnight at 4°C. Plates were washed 6 times with washing buffer (1× PBS with 0.05% Tween-20 (Sigma-Aldrich)) and incubated with 170 µl per well blocking buffer (1× PBS

with 2% BSA and 0.05% Tween-20 (Sigma)) for 1 hour at room temperature. Immediately after blocking, monoclonal antibodies or plasma samples were added in PBS and incubated for 1 hour at room temperature. Plasma samples were assayed at a 1:66 starting dilution and serially diluted by either three- or fourfold. Monoclonal antibodies were tested at 10 µg/ml starting concentration and 11 additional threefold serial dilutions. Plates were washed 6 times with washing buffer and then incubated with anti-human IgG or IgM secondary antibody conjugated to horseradish peroxidase (HRP) (Jackson Immuno Research 109-036-088 and 109-035-129) in blocking buffer at a 1:5,000 dilution (IgM and IgG). Plates were developed by addition of the HRP substrate, 3,3',5,5'-Tetramethylbenzidine (TMB) (ThermoFisher) for 6 minutes. The developing reaction was stopped by adding 50 µl of 1 M H_2SO_4 and absorbance was measured at 450 nm with an ELISA microplate reader (FluoStar Omega, BMG Labtech) with Omega and Omega MARS software for analysis. Normalizer control samples were included on each plate. For plasma samples and monoclonal antibodies half-maximal binding titers (BT50s) and half-maximal effective concentrations (EC50s), respectively, were calculated using four-parameter nonlinear regression (GraphPad Prism V9.3, with the following settings: [Agonist] vs. response -- Variable slope (four parameters), bottom=0, Hillslope>0, Top=plate/experiment-specific upper plateau of the normalizer control antibody/plasma reaching saturation for at least 3-consecutive dilution steps. The curve-fit was constrained to an upper limit that corresponds to the maximal optical density achieved by the known normalizer control to limit inter-plate-/experiment variability (batch effects). Pentameric IgM BT50s were established using previously measured IgG antibodies as normalizer controls. Pre-pandemic plasma samples from healthy donors and isotype control monoclonal antibodies served as negative controls as indicated and were used for validation (for more details see [5]). All reported EC50 and BT50 values are the average of at least 2 independent experiments.

Proteins

The mammalian expression vector encoding the Receptor Binding-Domain (RBD) of SARS-CoV-2 (GenBank MN985325.1; Spike (S) protein residues 319-539) was previously described[26]. Plasmids encoding the R346S/E484K and N440K/E484K substitutions, were generated using site-directed mutagenesis kit according to the manufacturer's instructions (New England Biolabs (NEB), E0554S). All constructs were confirmed by Sanger sequencing and used to express soluble

proteins by transiently transfecting Expi293F cells (GIBCO/Thermo Fisher, A14527)). Supernatants were harvested after four days, and RBD proteins were purified by nickel affinity chromatography. S 6P proteins were purified by nickel affinity following with size-exclusion chromatography. Peak fractions from size-exclusion chromatography were identified by native gel electrophoresis, and peak fractions corresponding to monomeric RBDs or spike trimers were pooled and stored at 4˚C.

SARS-CoV-2 pseudotyped reporter virus

A plasmid expressing SARS-CoV-2 spike (S) in the context of pSARS-CoV-2-S $_{\Delta 19}$ (Wuhan-Hu-1) has been described[6], and a derivative of pSARS-CoV-2-S $_{\Delta 19}$ with disrupted furin cleavage site was generated by introducing the R683G substitution[6]. Disruption of the furin cleavage site results in increased particle infectivity. A plasmid expressing SARS-CoV-2 Omicron BA.4/5 spike carrying the R683G substitution has been described earlier[38]. Two plasmids containing C135/C144 antibody escape mutations were constructed based on pSARS-CoV-2-S$_{\Delta 19}$ R683G by overlap extension PCR-mediated mutagenesis and Gibson assembly. Specifically, the substitutions introduced were: R346S/Q493K and R346S/N440K/E484K. Importantly, as those substitutions were incorporated into the pSARS-CoV-2-S$_{\Delta 19}$ R683G background, neutralizing activity against all mutant and variant pseudoviruses were compared to a wildtype (WT) SARS-CoV-2 spike sequence (NC_045512) also carrying R683G (pSARS-CoV-2-S$_{\Delta 19}$ R683G) where appropriate, as indicated. SARS-CoV-2 pseudotyped particles were generated as previously described[5,14]. Briefly, 293T cells were transfected with pNL4-3ΔEnv-nanoluc and pSARS-CoV-2-S$_{\Delta 19}$, particles were harvested 48 hours post-transfection, filtered and stored at -80°C.

Pseudotyped virus neutralization assay

Fivefold serially diluted pre-pandemic negative control plasma from healthy donors (technical negative controls, data not shown), plasma from vaccinated mAb recipients and mRNA vaccinated controls, or monoclonal antibodies were incubated with SARS-CoV-2 pseudotyped virus for 1 hour at 37 °C. The mixture was subsequently incubated with 293T$_{Ace2}$ cells[5] (for all monoclonal antibody WT neutralization assays) or HT1080Ace2 cl14 cells[6] (for all plasma neutralization assays) for 48 hours after which cells were washed with PBS and lysed with Luciferase Cell

Culture Lysis 5× reagent (Promega). Nanoluc Luciferase activity in lysates was measured using the Nano-Glo Luciferase Assay System (Promega) with the ClarioStar Multimode reader (BMG, software version 5.70.R3). The relative luminescence units were normalized to those derived from cells infected with SARS-CoV-2 pseudotyped virus in the absence of plasma or monoclonal antibodies. The half-maximal neutralization titers for plasma (NT_{50}) or half-maximal and 90% inhibitory concentrations for monoclonal antibodies (IC_{50} and IC_{90}) were determined using four-parameter nonlinear regression (least squares regression method without weighting; constraints: top=1, bottom=0; in GraphPad Prism).

Biotinylation of viral protein for use in flow cytometry and biolayer interferometry

Purified and Avi-tagged SARS-CoV-2 Wuhan-Hu-1 RBD or S were biotinylated using the Biotin-Protein Ligase-BIRA kit according to manufacturer's instructions (Avidity) as described before[5]. Ovalbumin (Sigma, A5503-1G) was biotinylated using the EZ-Link Sulfo-NHS-LC-Biotinylation kit according to the manufacturer's instructions (Thermo Scientific). Biotinylated ovalbumin was conjugated to streptavidin-BV711 for human single-cell sorts (BD biosciences, 563262) or to streptavidin-BB515 for phenotyping (BD biosciences, 564453). For all human and mouse experiments, RBD was conjugated to streptavidin-PE (BD Biosciences, 554061) and streptavidin-AF647 (Biolegend, 405237)[5,9].

Human flow cytometry and single cell sorting

Single-cell sorting by flow cytometry was described previously[5]. Briefly, peripheral blood mononuclear cells were enriched for B cells by negative selection using a pan-B-cell isolation kit according to the manufacturer's instructions (Miltenyi Biotec, 130-101-638). Prior to staining, the enriched B cells were incubated with an FcR-blocking antibody (BD 564220) at a 1:200 dilution in Flourescence-Activated Cell-sorting (FACS) buffer (1× PBS, 2% FCS, 1 mM ethylenediaminetetraacetic acid (EDTA)) for 20 min on ice. Subsequently, cells were incubated in FACS buffer with the following anti-human antibodies (all at 1:200 dilution): anti-CD20-PECy7 (BD Biosciences, 335793), anti-CD3-APC-eFluro 780 (Invitrogen, 47-0037-41), anti-CD8-APC-eFluor 780 (Invitrogen, 47-0086-42), anti-CD16-APC-eFluor 780 (Invitrogen, 47-0168-41), anti-CD14-APC-eFluor 780 (Invitrogen, 47-0149-42), as well as Zombie NIR (BioLegend, 423105) and fluorophore-labeled RBD and ovalbumin (Ova) for 30 min on ice. AccuCheck Counting Beads

(Life Technologies, PCB100) were added as indicated to each sample according to manufacturer's instructions. Single CD3-CD8-CD14-CD16−CD20+Ova−RBD-PE+RBD-AF647+ B cells were sorted into individual wells of 96-well plates containing 4 µl of lysis buffer (0.5× PBS, 10 mM Dithiothreitol (DTT), 3,000 units/ml RNasin Ribonuclease Inhibitors (Promega, N2615) per well using a FACS Aria III and FACSDiva software (Becton Dickinson) for acquisition and FlowJo for analysis. The sorted cells were frozen on dry ice, and then stored at −80 °C for subsequent RNA reverse transcription. For B cell phenotype analysis, in addition to above antibodies, B cells were also stained with following anti-human antibodies (all at 1:200 dilution): anti-CD19-BV605 (Biolegend, 302244), anti- IgG-PECF594 (BD, 562538), anti-IgM-AF700 (Biolegend, 314538), and anti-CD38-BV421 (Biolegend, 303526).

Mouse flow cytometry and single cell sorting

Popliteal lymph nodes from mice were collected in FACS buffer (1x PBS, 2% FBS, 2 mM EDTA), mechanically disrupted and filtered through a 35µM strainer (Corning, 352235). Cells then underwent iterative rounds of staining each for 20 minutes on ice (all antibodies diluted at 1:200 unless stated otherwise): 1) anti-mouse CD16/32 (Mouse BD FC Block™, BD Biosciences, 553142); 2) fluorophore-conjugated RBD (see above); 3) anti-T and -B cell activation antigen-FITC (BD Biosciences, 553666), anti-CD38-PB (Biolegend, 102720; 1:100 dilution), anti-CD45R/B220-BV605 (Biolegend, 103244), anti-CD4-APC-eFluor780 (Invitrogen, 47-0042-82), anti-CD8a-APC-eFluor780 (Invitrogen, 47-0081-82), anti-NK1.1-APC-eFluor780 (Invitrogen, 47-5941-82), anti-F4/80-APC-eFluor780 (Invitrogen, 47-4801-82), anti-CD95-PE-Cy7 (BD Biosciences, 557653) and Zombie NIR (Biolegend, 423105, 1:1000 dilution). AccuCheck Counting Beads (Life Technologies, PCB100) were added to samples according to the manufacturer's instructions. Single CD4-CD8a-NK1.1-F4/80-B220+CD38-GL7+CD95+ cells were sorted on a BD FACSymphony S6 into 96 well plates containing 1% 2-β-mercaptoethanol (Sigma) in TCL Buffer (Qiagen, 1031576) and subsequently frozen on dry ice and stored at −80 °C for RNA reverse transcription.

Antibody sequencing, cloning and expression

Human antibodies were identified and sequenced as described previously[5,39]. In brief, RNA from single cells was reverse-transcribed (SuperScript III Reverse Transcriptase, Invitrogen, 18080-

044) and the cDNA was stored at −20 °C or used for subsequent amplification of the variable IGH, IGL and IGK genes by nested PCR and Sanger sequencing. Sequence analysis was performed using MacVector (version 17.5.4) and Geneious Prime (versions 2020.1.2 and 2022.1.1). Amplicons from the first PCR reaction were used as templates for sequence- and ligation-independent cloning into antibody expression vectors. Mouse monoclonal antibodies were sequenced and cloned from single FACS-sorted B cells as previously described[40,41] with the following modifications. In brief, RNA from single cells in 96-well plates was purified using magnetic beads (RNAClean XP, Beckman Coulter, Cat # A63987). Single-cell RNA was eluted from magnetic beads with 11 µL of solution containing 14.4 ng/µL of random primers (Invitrogen, Cat #48190011), 0.5% of IGEPAL CA-630 (10% in dH2O, Sigma-Aldrich, Cat I8896-50ML) and 0.6 U/µL of RNase inhibitor (Promega, Cat# N2615) in nuclease-free water (Qiagen, Cat# 129115), followed by incubation at 65 °C for 3 min. cDNA was synthesized by reverse transcription (SuperScript III Reverse Transcriptase 10,000 U, Invitrogen, Cat# 18080-044) and stored at −20 °C after addition of 10 µL nuclease-free water. Subsequent amplification of the variable IGH and IGK antibody genes was achieved by nested polymerase chain reaction (PCR) using HotstarTaq DNA polymerase (Qiagen Cat # 203209), using previously published primers[41] and the following thermocycler conditions for annealing (°C)/elongation (s)/number of cycles: PCR1 (IgG, IgM and IgK): 46/55/50; PCR2 (IgG and IgM): 55/55/50; PCR2 (IgK): 46/55/50. After purification, HC and LC PCR products were Sanger sequenced, and subsequently analyzed using MacVector and Geneious Prime (version 2022.1.1), as well as the bioinformatics pipeline detailed below. Mouse Ig sequences were ordered as eBlocks (IDT) with short homologies for Sequence and Ligation Independent Cloning (SLIC) and cloned into human IGHG1 Fab and IGLK expression vectors as previously described[41]. All plasmid sequences were verified by Sanger sequencing, and all recombinant monoclonal antibodies (human memory B cell derived full-length IgG and His_6-tagged mouse-derived human IgG1 Fabs) were thereafter produced and purified as previously described[5,41]. To produce pentameric IgMs, cloning from PCR products was performed by sequencing and ligation-independent cloning (SLIC) as above, except that the IGH variable gene was cloned into an Igµ expression vector (InvivoGen, cat# pfusess-hchm3). Pentameric IgMs were then expressed via transient transfection of HEK293-6E cells with vectors encoding the appropriate J chain, light chain, and heavy chain at a ratio of 1:1.5:1.5. Secreted IgMs were collected from cell supernatants after 6 days and purified with the POROS CaptureSelect IgM

Affinity Matrix kit (Thermo Scientific Cat#1952890500). Affinity-purified IgMs were further purified via size exclusion chromatography. Peak fractions of pentameric IgMs were analyzed by SDS-PAGE, pooled, and buffer exchanged into phosphate buffered saline using an Amicon Ultra 100kDa (Millipore) centrifugal filter unit.

Biolayer interferometry

Biolayer interferometry assays were performed as previously described[5,15,41] with minor modifications as below. Briefly, we used the ForteBio Octet Red instrument (ForteBio Data Acquisition software version 11.1.3.25) at 30 °C with shaking at 1,000 r.p.m.. Monomeric affinities of anti-SARS-CoV-2 RBD IgG and Fabs to RBD were derived by subtracting the signal obtained from traces performed with the same IgG/Fab in the absence of WT RBD. Kinetic analysis using protein A biosensor (ForteBio, 18-5010) for human IgGs was performed as follows: (1) baseline: immersion for 60 s in buffer (1X Octet Kinetic buffer, Sartorius 18-1105); (2) loading: immersion for 200 s in a solution with IgGs at 10 μg ml–1; (3) baseline: immersion for 200 s in buffer; (4) association: immersion for 300 s in solution with WT RBD at three different concentrations ranging from 200 to 5 μg ml–1; (5) dissociation: immersion for 600 s in buffer. Curve fitting was performed using a fast 1:1 binding model and the data analysis software from ForteBio. Mean equilibrium dissociation constants (Kd) were determined by averaging all binding curves that matched the theoretical fit with an R2 value ≥0.8. To establish binding of low-affinity antibodies to multimerized antigen, 6P-stabilized and biotinylated S trimers were incubated with recombinant Streptavidin (ACROBiosystems, cat# STN-N5116) for 30 min at RT, resulting in up to 12 RBD-binding moieties per molecule and assayed on the Octet Red instrument (ForteBio) as above, with the following modification: Association step (4) was performed with the S-multimer at 430 μg ml–1. Epitope mapping assays were performed with protein A biosensor (ForteBio 18-5010), following the manufacturer's protocol "classical sandwich assay" as follows: (1) Sensor check: sensors immersed 30 sec in buffer alone (buffer ForteBio 18-1105), (2) Capture 1st Ab: sensors immersed 10 min with Ab1 at 10 μg ml–1, (3) Baseline: sensors immersed 30 sec in buffer alone, (4) Blocking: sensors immersed 5 min with IgG isotype control (3BNC117) at 20 μg ml–1. (5) Baseline: sensors immersed 30 sec in buffer alone, (6) Antigen association: sensors immersed 5 min with RBD at 20 μg ml–1. (7) Baseline: sensors immersed 30 sec in buffer alone. (8) Association Ab2: sensors immersed 5 min with Ab2 at 10 μg ml–1. Affinity testing of mouse GC

B cell-derived human IgG1 Fabs was performed using the same steps and Octet Red instrument (ForteBio) settings as for the human memory-derived full-length IgG antibodies (see above) with the following modifications: Monoclonal Fabs at 50 µg ml–1 were captured on FAB2G biosensors (Sartorius 18-5125) for step (2); monovalent RBD was added at concentrations ranging from 30 to 120 µg ml–1 in step (4). Binding Fabs with measurable affinities were defined as having biologically plausible association and dissociation kinetics (i.e., being able to associate to saturation on the biosensor in step (2) and showing a discernible association and dissociation of antigen upon steps (4) and (5)) as well as a computed Kd value that matched the theoretical fit with an R2 value of ≥0.75. Affinities of Fabs that did not get captured on the biosensor to saturation at the concentration tested could not be resolved and were excluded from further analysis (marked as N/D in Supplementary Table 6). In all cases, curve fitting was performed using the ForteBio Octet Data analysis software (ForteBio Data Analysis HT version 11.1.3.50).

Computational analyses of antibody sequences

Antibody sequences were trimmed based on quality and annotated using Igblastn v.1.14. with IMGT domain delineation system. Annotation was performed systematically using Change-O toolkit v.0.4.540[42]. Clonality of heavy and light chain was determined using DefineClones.py implemented by Change-O v0.4.5[42]. The script calculates the Hamming distance between each sequence in the data set and its nearest neighbor. Distances are subsequently normalized and to account for differences in junction sequence length, and clonality is determined based on a cut-off threshold of 0.15. Heavy and light chains derived from the same cell were subsequently paired, and clonotypes were assigned based on their V and J genes using in-house R and Perl scripts. All scripts and the data used to process antibody sequences are publicly available on GitHub (https://github.com/stratust/igpipeline/tree/igpipeline2_timepoint_v2). The frequency distribution of human V genes in anti-SARS-CoV-2 antibodies from this study (Ext. Data Fig. 4f-h) was compared to 131,284,220 IgH and IgL sequences generated by Soto et al.[43] and downloaded from cAb-Rep[44], a database of human shared BCR clonotypes available at https://cab-rep.c2b2.columbia.edu/. Based on the 108 distinct V genes that make up the 417 analyzed sequences from the Ig repertoire of the individuals described in this study (353 sequences isolated form 5 monoclonal antibody recipients and 65 IgM sequences isolated from 9 vaccinated control

individuals (for IgG sequences isolated from controls see [9,11]), we selected the IgH and IgL sequences from the database that are partially coded by the same V genes and counted them according to the constant region. The frequencies shown in Ext. Data Fig. 4f-h are relative to the source and isotype analyzed. We used the two-sided binomial test to check whether the number of sequences belonging to a specific IGHV or IGLV gene in the repertoire is different according to the frequency of the same IgV gene in the database. Adjusted p-values were calculated using the false discovery rate (FDR) correction. Significant differences are denoted with stars. Nucleotide somatic mutations and Complementarity-Determining Region (CDR3) length were determined using in-house R and Perl scripts. For quantification of somatic mutations, *IGHV* and *IGLV* nucleotide sequences were aligned against their closest germlines using Igblastn and the number of differences were considered nucleotide mutations.

Data presentation

Figures arranged in Adobe Illustrator 2022.

Data availability statement:

Data are provided in Supplementary Tables 1-6. The raw sequencing data and computer scripts associated with Figs. 2 and 4, and Ext. Data Figs. 3 and 7 have been deposited at Github (https://github.com/stratust/igpipeline/tree/igpipeline2_timepoint_v2). This study also uses data from "A Public Database of Memory and Naive B-Cell Receptor Sequences" (https://doi.org/10.5061/dryad.35ks2), PDB (6VYB and 6NB6), cAb-Rep (https://cab-rep.c2b2.columbia.edu/), Sequence Read Archive (accession SRP010970), and from "High frequency of shared clonotypes in human B cell receptor repertoires" (https://doi.org/10.1038/s41586-019-0934-8).

Code availability statement:

Computer code to process the antibody sequences is available at GitHub (https://github.com/stratust/igpipeline/tree/igpipeline2_timepoint_v2).

Additional references

36 Amanat, F. *et al.* A serological assay to detect SARS-CoV-2 seroconversion in humans. *Nat Med* **26**, 1033-1036, doi:10.1038/s41591-020-0913-5 PMID - 32398876 (2020).

37 Grifoni, A. *et al.* Targets of T Cell Responses to SARS-CoV-2 Coronavirus in Humans with COVID-19 Disease and Unexposed Individuals. *Cell* **181**, 1489-1501.e1415, doi:10.1016/j.cell.2020.05.015 PMID - 32473127 (2020).

38 Wang, Z. *et al.* Memory B cell responses to Omicron subvariants after SARS-CoV-2 mRNA breakthrough infection in humans. *The Journal of experimental medicine* **219**, doi:10.1084/jem.20221006 (2022).

39 Wang, Z. *et al.* Enhanced SARS-CoV-2 neutralization by dimeric IgA. *Sci Transl Med* **13**, doi:10.1126/scitranslmed.abf1555 (2021).

40 Escolano, A. *et al.* Immunization expands B cells specific to HIV-1 V3 glycan in mice and macaques. *Nature* **570**, 468-473, doi:10.1038/s41586-019-1250-z PMID - 31142836 (2019).

41 Viant, C., Escolano, A., Chen, S. T. & Nussenzweig, M. C. Sequencing, cloning, and antigen binding analysis of monoclonal antibodies isolated from single mouse B cells. *STAR Protoc* **2**, 100389, doi:10.1016/j.xpro.2021.100389 (2021).

42 Gupta, N. T. *et al.* Change-O: a toolkit for analyzing large-scale B cell immunoglobulin repertoire sequencing data. *Bioinformatics* **31**, 3356-3358, doi:10.1093/bioinformatics/btv359 PMID - 26069265 (2015).

43 Soto, C. *et al.* High frequency of shared clonotypes in human B cell receptor repertoires. *Nature* **566**, 398-402, doi:10.1038/s41586-019-0934-8 PMID - 30760926 (2019).

44 Guo, Y., Chen, K., Kwong, P. D., Shapiro, L. & Sheng, Z. cAb-Rep: A Database of Curated Antibody Repertoires for Exploring Antibody Diversity and Predicting Antibody Prevalence. *Front Immunol* **10**, 2365, doi:10.3389/fimmu.2019.02365 PMID - 31649674 (2019).

Acknowledgements:

We thank all study participants who devoted their time to our research; The Rockefeller University Hospital nursing staff and Clinical Research Support Office and nursing staff; all members of the M.C.N. laboratory for helpful discussions; M. Jankovic and G. Scrivanti for laboratory support; T. Eisenreich for help with mouse colony management and technical help; K. Gordon for cell sorting. This work was supported by NIH grants P01-AI138398-S1 and 2U19-AI111825 to M.C.N., R37-AI64003 to P.D.B. and R01-AI78788 to T.H., and 3UM1AI126620-5S1 to M. Caskey. D.S.-B. is supported in part by the National Center for Advancing Translational Sciences (NIH Clinical and Translational Science Award program, grant UL1-TR001866) and the Shapiro–Silverberg Fund for the Advancement of Translational Research. F.M. was supported by the Bulgari Women & Science Fellowship in COVID-19 Research. P.D.B. and M.C.N. are Howard Hughes Medical

Author Contributions:

D.S.-B. and M.C.N. conceptualized the study. D.S.-B., Z.W., F.M., A.C., P.D.B., T.H., and M.C.N. conceived, designed and analyzed experiments. D.S.-B., C.G., and M. Caskey designed clinical protocols. D.S.-B., Z.W., F.M., A.C., M.L., M.C., R.R., M. Canis, J.DaSilva., F.S., L.W. and K.Y. carried out experiments. B.J. and A.G. produced antibodies. M.T., K.G.M., I.S., J.Dizon, C.G. and M.Caskey recruited participants, executed clinical protocols, and processed samples. V.R. and T.Y.O. performed bioinformatic analysis. D.S.-B. and M.C.N. wrote the manuscript with input from all co-authors.

Competing interests

The Rockefeller University has filed a provisional patent application in connection with this work, on which M.C.N. is an inventor (US patent 63/021,387). The patent has been licensed by Rockefeller University to Bristol Meyers Squib. P.D.B. has received remuneration from Pfizer for consulting services related to SARS-CoV-2 vaccines.

Extended Data Figures

Extended Data Fig. 1: C135 and C144 – selectively abrogated binding to mutant RBDs and correlations with plasma reactivity.

a-f, Monoclonal antibody binding to mutant forms of RBD. **a-c**, Graphs show concentration-dependent antibody binding to (**a**) WT, (**b**) R436S/E484K, and (**c**) N440K/E484K RBDs by C144, C135, and Class 1 (C105), Class 2 (C952), Class 3 (C881), and Class 4 (C149)[5,6,8,26]. **d-f**, Graphs show concentration dependent pre-pandemic healthy donor plasma binding to (**d**) WT, (**e**) R436S/E484K, and (**e**) N440K/E484K RBDs in the presence (purple) or absence (dotted lines) of 100mg/ml of C135 and C144. Addition of C144 and C135 to plasma increases the binding activity of plasma against the WT but not the 2 mutant RBDs. **g-h**, Panels show the correlation of C135-LS (**g**) and C144-LS (**h**) serum levels at day 84 post-administration (around the times of vaccination as seen in Fig. 1b) with the total anti-WT RBD IgG antibody titers of mAb recipients (n=18) after one (empty green circles) and two doses (solid green dots) of mRNA vaccination. Statistical significance in **g** ($r= 0.9097$ and $r=0.5891$ with $p<0.0001$ and $p=0.0101$ for vax1 and vax2, respectively) and **h** ($r= 0.8772$ and $r=0.5483$ with $p<0.0001$ and $p=0.0185$ for vax1 and vax2, respectively) was determined using the two-tailed Pearson correlation statistic. All experiments were performed at least in duplicate.

Extended Data Fig. 2: SARS-CoV-2 R346S/Q493K and R346S/N440K/E484K pseudotype virus neutralization by C135-LS and C144-LS, and BA.4/5 pseudotype neutralization by plasma.

a, Graphs show concentration-dependent neutralization curves for SARS-CoV-2 pseudoviruses by monoclonal antibodies. C144 (red), C135 (blue), and their equimolar combination (purple). **b,** Pre-pandemic plasma (squares) neutralization of WT or R346S/Q493K or R346S/N440K/E484K pseudoviruses in the absence or presence of 5 (purple dashed circles) or 100µg/ml (purple solid circles) of C135 and C144[14]. **c-d,** As in (**b**) but for convalescent plasma with intermediate (**c**, COV157) [12] or strong (**d**, COV31)[12] neutralizing activity. The horizontal lines in all panels indicate half-maximal neutralization. **e**, Plasma half-maximal neutralizing titers (NT50s) against HIV-1 pseudotyped with the BA.4/5 S[38]. Each dot represents one individual from the control group (n=31, blue) or from the mAb recipient group (n=18, green). Red horizontal bars and red numbers represent median values. Statistical significance was determined using the two-tailed Mann-Whitney. For **a-d**, individual symbols represent the mean of two independent experiments and error bars the standard deviation. All experiments were performed at least in duplicate.

Extended Data Fig. 3: Flow-cytometry of human anti-RBD memory B cells.

a, Gating strategy for flow-cytometry phenotyping. Gating was on single lymphocytes that were $CD19^+$ and $CD20^+$, and $CD3^-$ $CD8^-$ $CD16^-$ Ova^- without uptake of live-dead dye (L/D). Antigen-specific cells were those with dual binding to Wuhan-Hu1 RBD-PE and RBD-AF647. Anti-IgG, -IgM were used to phenotype dual RBD-labelled B cells. **b,c,** Representative flow-cytometry plots of Wuhan Hu-1 RBD-binding memory B cells from mAb recipients after one and two doses of vaccination (**b**) and pre-pandemic health donors (**c**) serving as negative controls. Numbers in RBD-gate denote percentage of RBD dual-labelled cells of parent gate (see **a**). Corresponding flow-cytometry plots and gating strategy for vaccinated controls can be found in [11]. **d-e,** Number of IgG- (**d**) and IgM-expressing (**e**) WT RBD-specific memory B cells per 10 million $CD20^+$ B cells. Each dot represents one individual from the mAb recipient (green, n=18) and control group (blue, n=10)[9,11]. Horizontal red bars denote median values. **f-i,** Panels show the correlation of C135-LS (**f, g**) and C144-LS (**h,i**) serum levels at day 84 post-administration (around the times of vaccination as seen in Fig. 1b) with the percentage of WT RBD-specific memory B cells expressing either IgG (**f, h**) or IgM (**g, i**) after two vaccine doses as assessed by flow-cytometry. Green dots represent individual mAb recipients (n=18). Statistical significance was determined using the two-tailed Mann-Whitney for **d** and **e**, and the Pearson r correlation statistic was used for **f-i**.

Extended Data Fig. 4: Fluorescence-activated cell sorting (FACS) of human anti-RBD memory B cells and subsequent BCR sequencing.

a-b, Panels showing IgG (**a**) and IgM (**b**) surface expression of anti-RBD memory cells exactly as in Fig. 2b and c, but with the 5 representative individuals from whom cells were subsequently sorted highlighted in yellow. **c,** Gating strategy for single-cell sorting of RBD-specific memory B cells. Dual-labelled (RBD-PE^+/-$AF647^+$) $CD20^+$ $CD3^-$ $CD8^-$ $CD16^-$ Ova^- cells were sorted. **d,** Representative flow cytometry plots show RBD-binding cells that were sorted from the 5 mAb recipients. **e,** Pie charts show the distribution of antibody sequences derived from cells isolated from 10 vaccinated control individual after vax2. The upper panel shows IgM, and the lower panel depicts IgG sequences[9,11]. The number in the inner circle indicates the number of sequences analyzed for the individual denoted above the circle. Slices colored in shades of blue indicate cells that are clonally expanded (same IGHV and IGLV genes, with highly similar CDR3s). Pie slice size is proportional to the number of clonally related sequences. The black outline and % value indicate the frequency of clonally expanded sequences detected within an individual. White pie areas indicate the proportion of sequences isolated only once. For C005, there were no IgM transcripts amplified at the timepoint assayed. **f-h,** Comparison of the frequency distribution of V gene usage for the IgH and IgL among antibodies isolated from mRNA-vaccinated mAb recipients (this study) and controls[9,11], after vax2, and from database of shared clonotypes of human antibodies from Soto et al[43]. Graphs show relative abundance of human IGHV (**f**), IGKV (**g**), and IGLV (**h**) genes within the human V

gene database (in grey, Sequence Read Archive accession SRP010970), antibodies isolated from mAb recipients (in green) or vaccinated controls (in blue). Colors of stars indicate levels of statistical significance for the following frequency comparisons: black – vaccinated controls vs. database; red – mAb recipients vs. database; blue – mAb recipients vs. vaccinated controls.

Extended Data Fig. 5: WT RBD binding and WT SARS-Cov-2 neutralization by monoclonal pentameric IgM antibodies.

a-b, Panels depict WT RBD binding and WT SARS-CoV-2 S pseudotype neutralizing activity of a representative panels of monoclonal antibodies derived from IgM-expressing RBD-specific memory B cells expressed either as human IgG1 (IgG, as in Fig. 3a-c) or pentameric IgM (IgM^5). **a,** Panel shows WT RBD EC50s of 15 monoclonal antibodies isolated from vaccinated mAb recipients (also see Supplementary Table 4). Grey shaded area between horizontal dotted lines indicates antibodies with EC50s >10 μg/ml (poor binding) and non-binding antibodies arbitrarily grouped at 10 and 20 μg/ml, respectively. **b,** Plots show IC50s of 2 IgM-derived control antibodies (covering a wide range of neutralizing activity) in blue and 15 IgM-derived monoclonal antibodies from mAb recipients (as in **a**) in green, expressed as human IgG1 (IgG) or pentameric IgM (IgM^5). For both panels (**a, b**), ring plots summarize the fraction of antibodies in the indicated category among all tested (encircled number). Red horizontal bars and numbers indicate median values. For panel **a**, statistical significance was determined using the two-tailed Wilcoxon matched-pairs rank test to compare differences between the same monoclonal antibodies expressed as IgG or pentameric IgM, and the Chi-squared contingency statistic was used to compare categorical distributions from ring plots.

Extended Data Fig. 6: Competition BLI.

a-d, BLI traces of antibodies assayed for competition with class-reference antibodies. Traces show initial association curve (antigen capture phase of the primary antibody) and subsequent addition of secondary antibodies of unknown class. Thin solid black lines represent antibodies isolated from mAb recipients or vaccinated controls. Thick dashed lines are self-competition traces of C105 (green in **a**), C144 (red in **b**), C135 (blue in **c**) and C2172 (purple in **d**) for classes 1-4, respectively. **e,** Heat-map of relative inhibition of secondary antibody binding to the preformed capture antibody-RBD complexes (grey=no binding, red=unimpaired binding, orange=indeterminate). The left panel shows antibodies from mAb recipients, while the right panel shows IgM antibodies from vaccinated controls isolated in this study (both after vax2). Details on IgG antibodies isolated from vaccinated controls can be found in [9,11]. **f,** BLI traces defining C2172 as Class 4. C2172 is the primary/capture antibody (in dashed purple). The addition of known class-

defining antibodies C105 (in green, Class 1[8]), C144 (in red, Class 2[8]), C135 (in blue, Class 3[8]), and C118 (in orange, Class 1/4[27]) establish C2172 as a bona fide Class 4 antibody.

Extended Data Fig. 7: Flow-cytometry of germinal center (GC) responses in mAb pre-treated mice and molecular characterization of GC-derived monoclonal antibodies.

a, Gating strategy for flow-cytometry phenotyping of germinal center (GC) B cells isolated from the draining (popliteal) lymph nodes of wildtype C57BL/6 mice immunized with recombinant SARS-Cov-2 RBD 11 days prior (as illustrated in Fig. 4a). Gating was on single lymphocytes that were $B220^+$ and $CD4^-$ $CD8a^-$ $NK1.1^-$ $F4/80^-$ (lineage-negative) without uptake of live-dead dye (L/D). GC B cells were those that were $CD38^-$ $GL7^+$ CD95 $(Fas)^+$. Antigen-specific cells were those with dual binding to Wuhan-Hu1 RBD-PE and RBD-AF647. **b,** Representative flow-cytometry plots of Wuhan Hu-1 RBD-binding GC B cells from mice that had either received the combination of C135 and C144 (anti-RBD mAb group) or the irrelevant anti-HIV control antibodies 3BNC117 and 10-1074 (anti-HIV mAb controls) one day prior to immunization, with the percentage of binding cells denoted within the respective gate. **c-d**, Panels show the total number of $CD38^-$ $GL7^+$ CD95 $(Fas)^+$ GC B cells (**c**) and RBD-binding GC B cells (**d**) isolated from anti-RBD mAb pre-treated (n=6, green) and control mice (n=6, blue), with each dot corresponding to an individual mouse. **e**, Somatic hypermutation (SHM) levels of GC B cell-derived monoclonal antibodies shown as combined heavy- and light-chain variable region nucleotide substitutions plus one (IGVH+IGVL+1), with each dot representing one sequence from anti-RBD mAb pre-treated mice (green) or controls (blue). Ring plots below each column show the fraction of sequences with no (IGVH+IGVL+1 = 1) vs. any (IGVH+IGVL+1 > 1) SHM among all sequences analyzed (encircled number) for the respective group. **f,** Percentage of sequences belonging to clones, defined as 2 or more sequences with the same IGHV and IGLV genes and with highly similar CDR3s, among all sequences obtained from the respective animal (as in Fig. 4d). Each dot represents one individual mouse from the anti-RBD mAb (n=6, green) or control group (n=6, blue). **g**, Affinity constants (K_d) of GC B cell-derived Fabs for WT SARS-CoV-2 RBD, as established from the monovalent interaction of Fabs with RBD monomers by biolayer interferometry (BLI, also see Fig. 4f-i, Supplementary Table 6 and methods). Each dot represents a single Fab from the anti-RBD mAb (n=8, green) or control group (n=22, blue). Red horizontal bars (**c-g**) and numbers (**e, g**) indicate median (**c, d, f, g**) and mean (**e**) values. Statistical significance was determined using the two-tailed Mann-Whitney test for **c-g d**, and the two-sided Fisher's exact test was used to test the relative contribution of mutated and unmutated sequences in **e**.

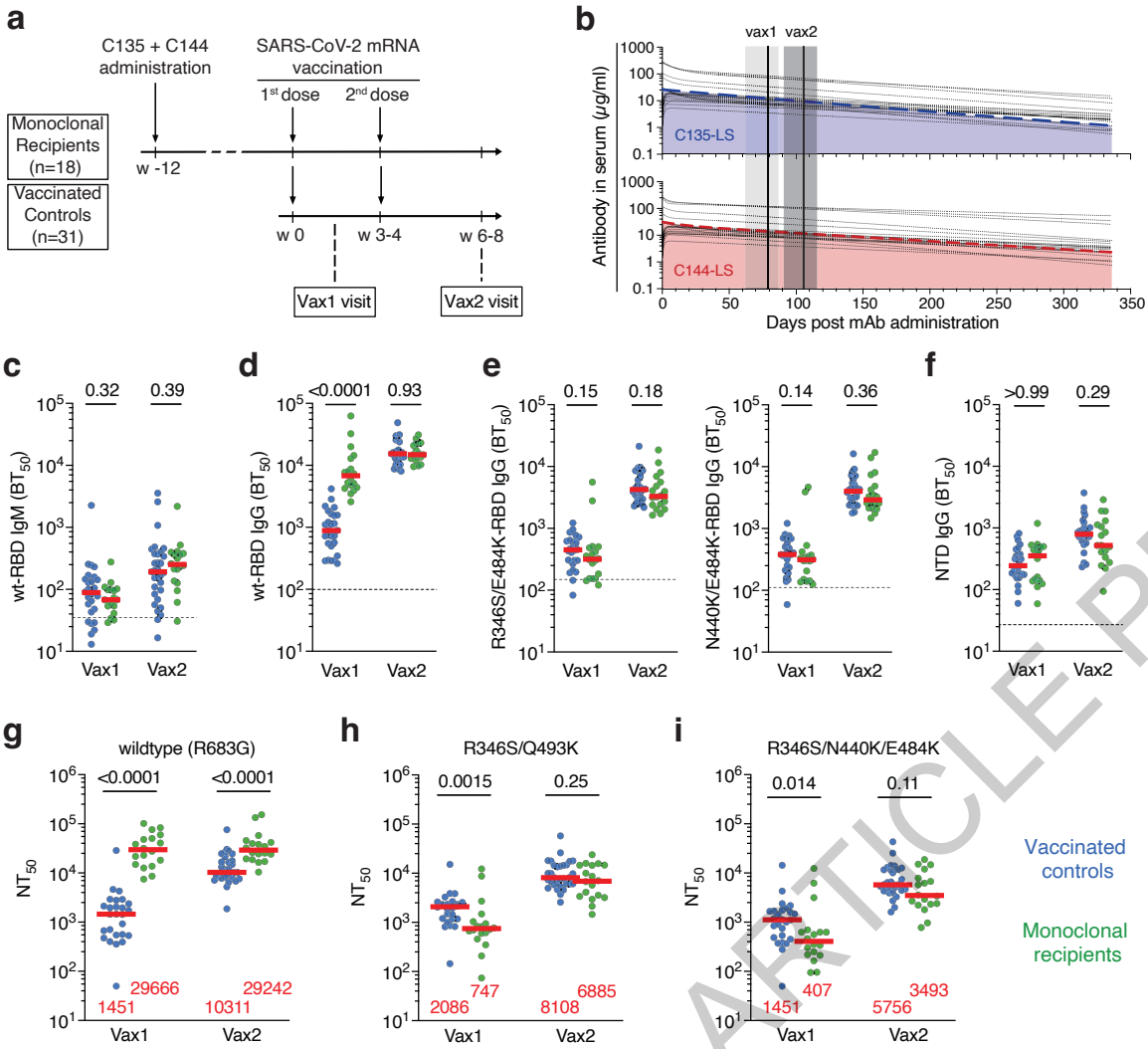

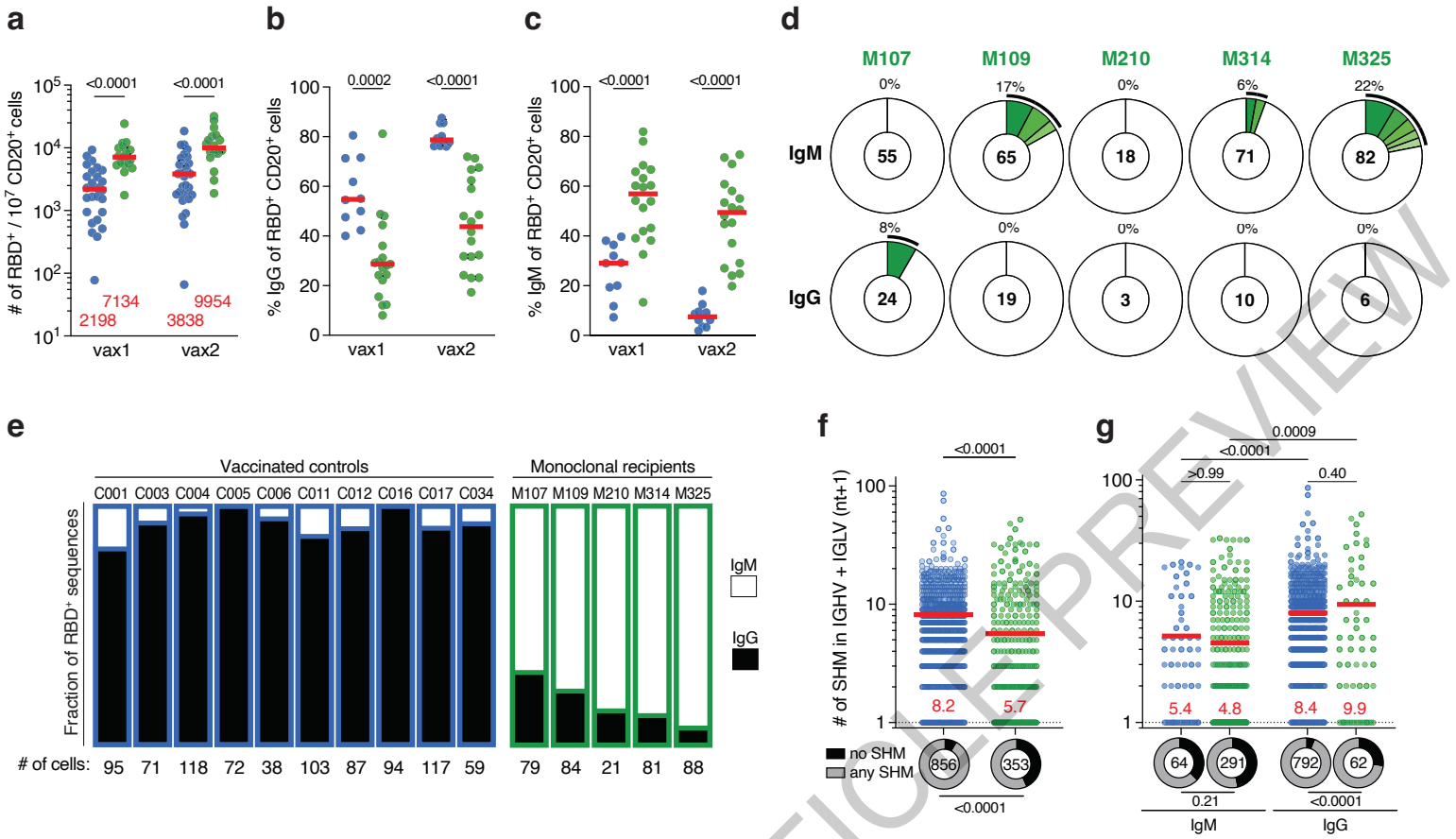

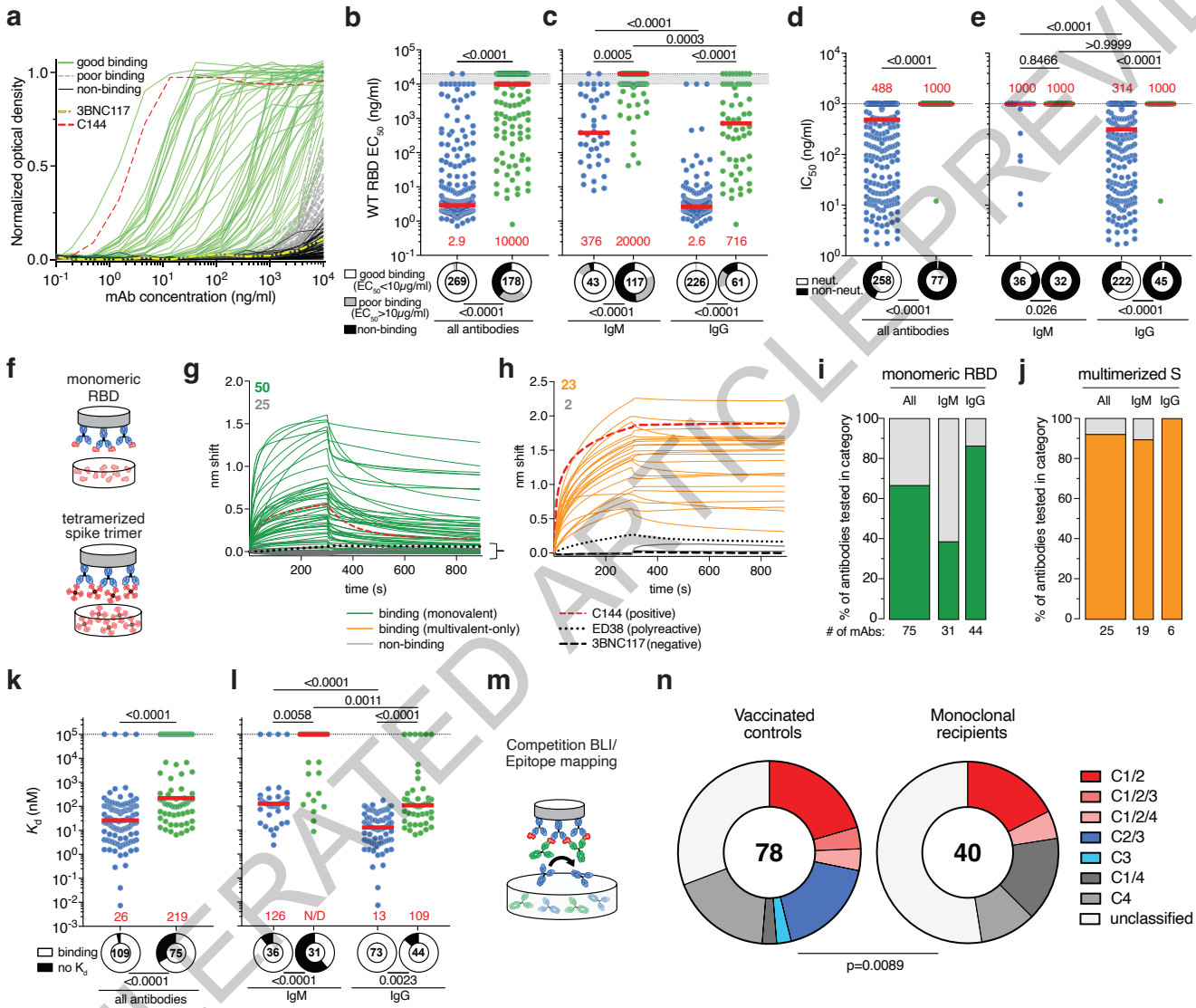

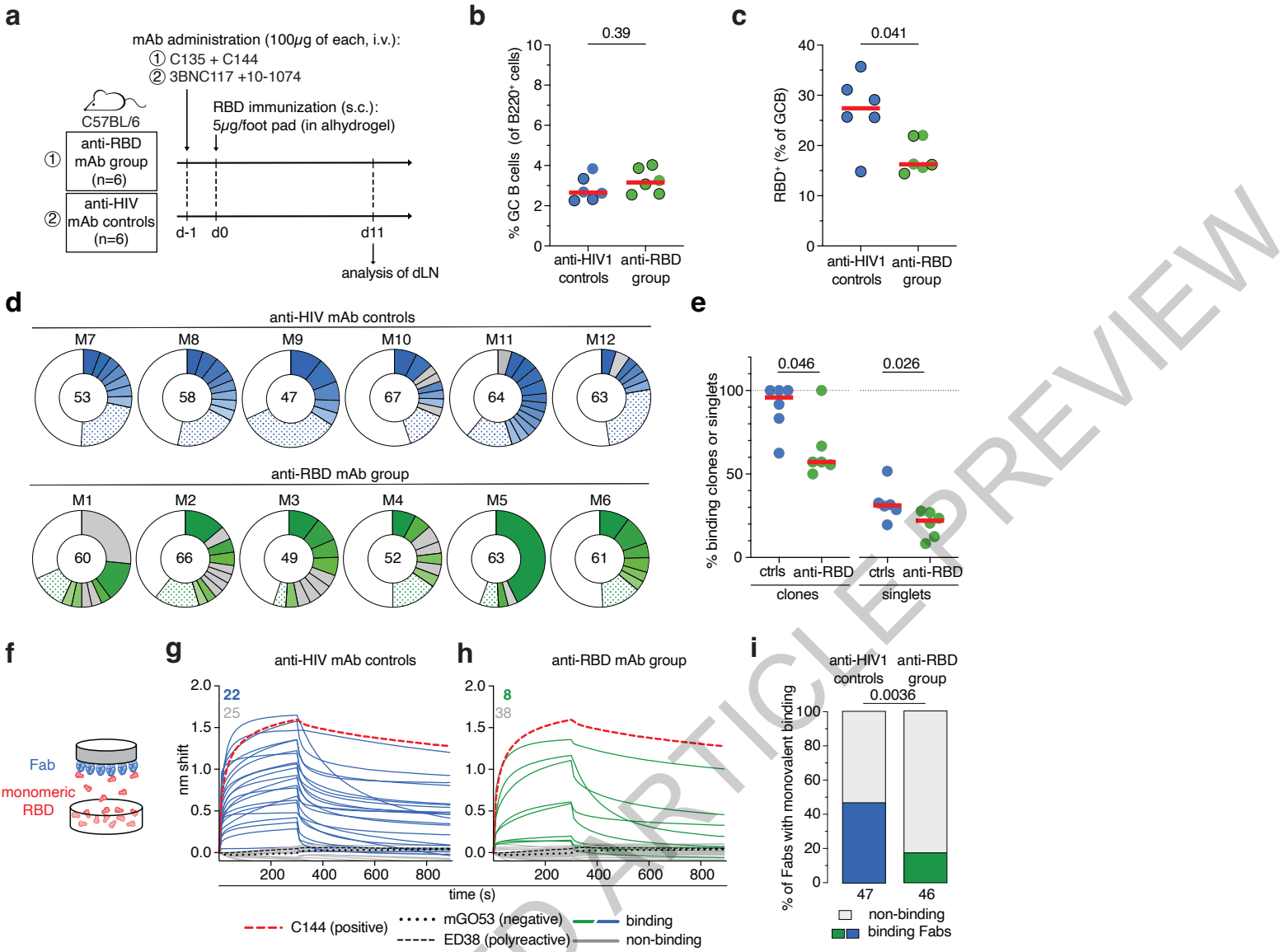

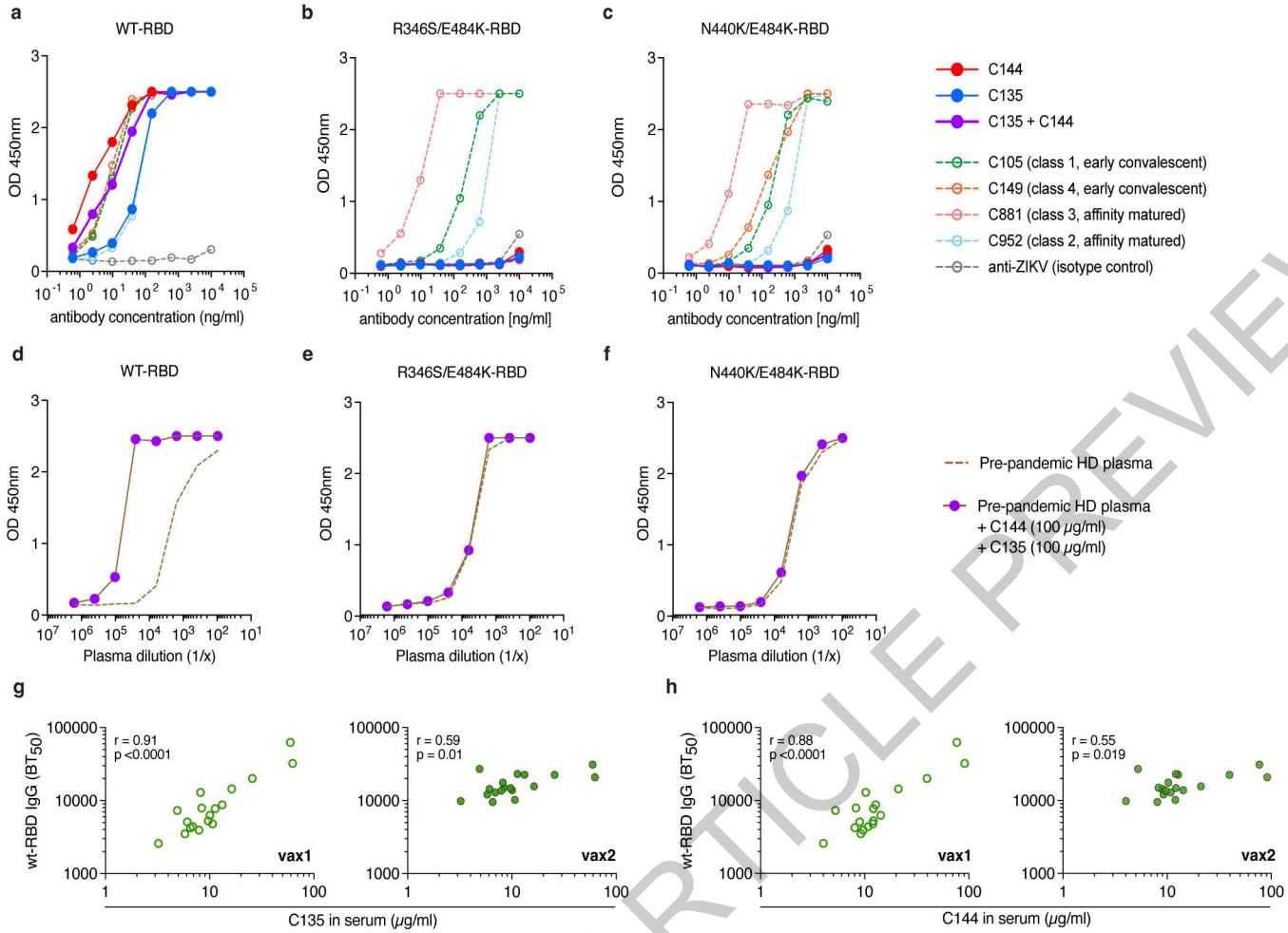

Extended Data Fig.1

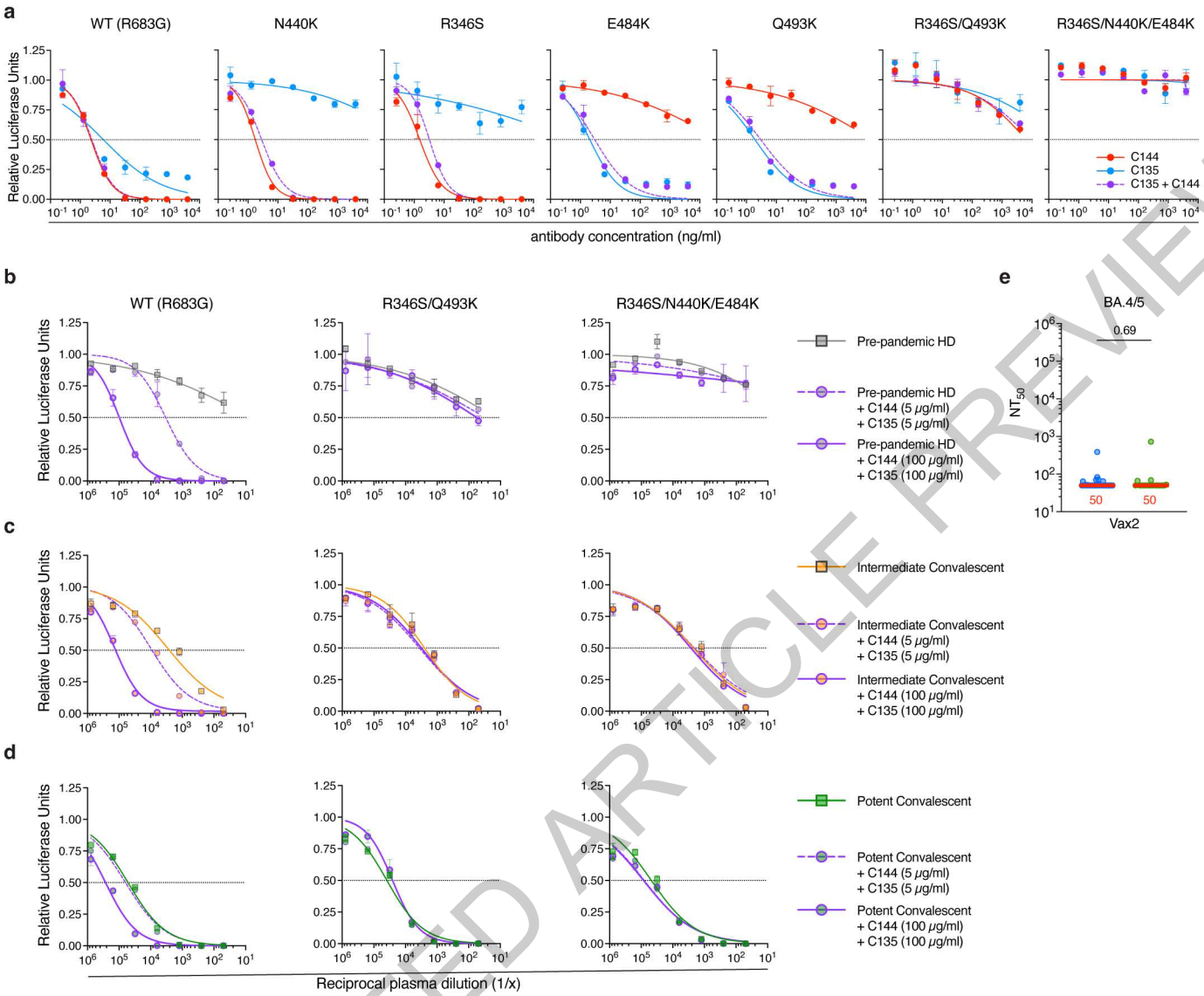

Extended Data Fig.2

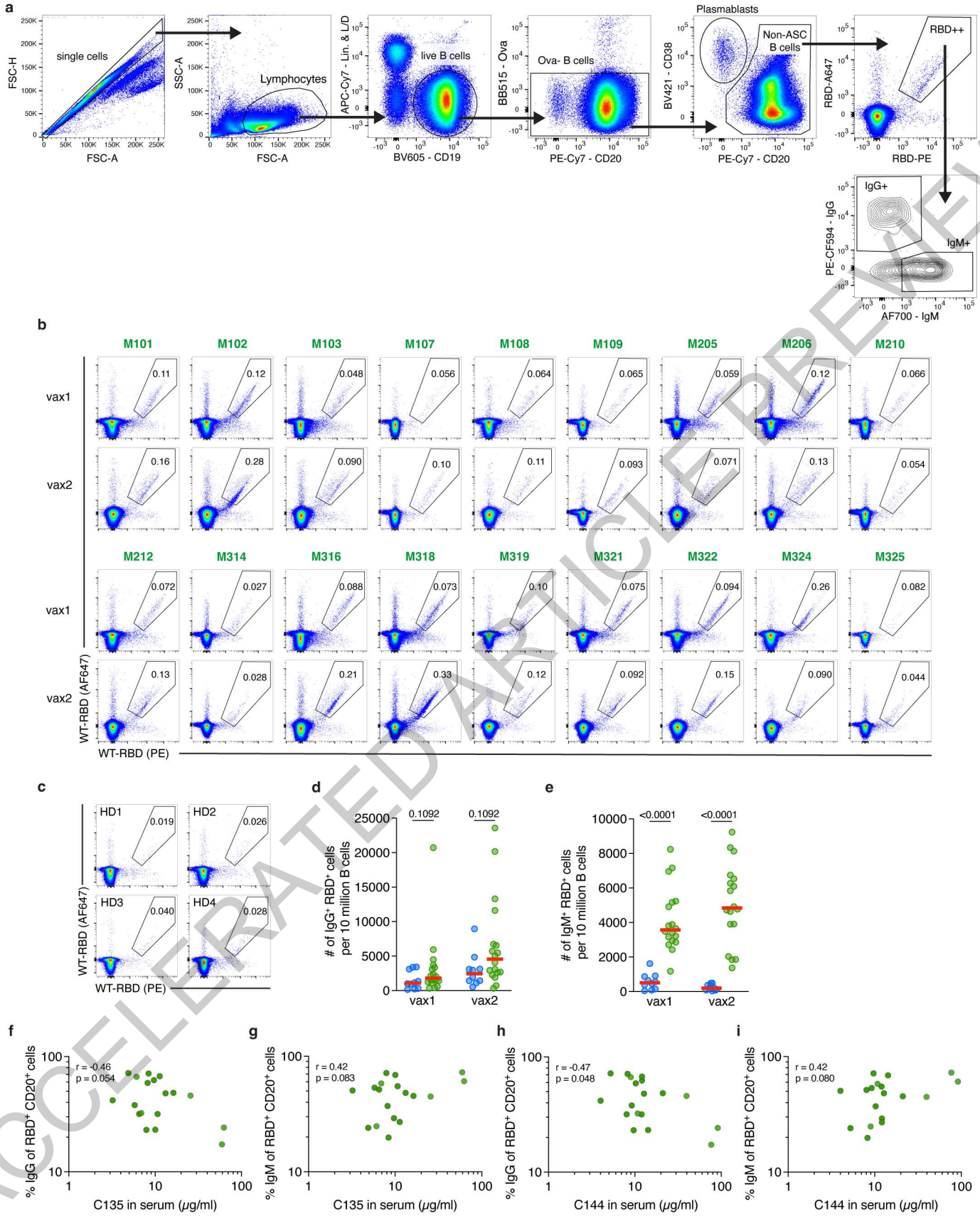

Extended Data Fig.3

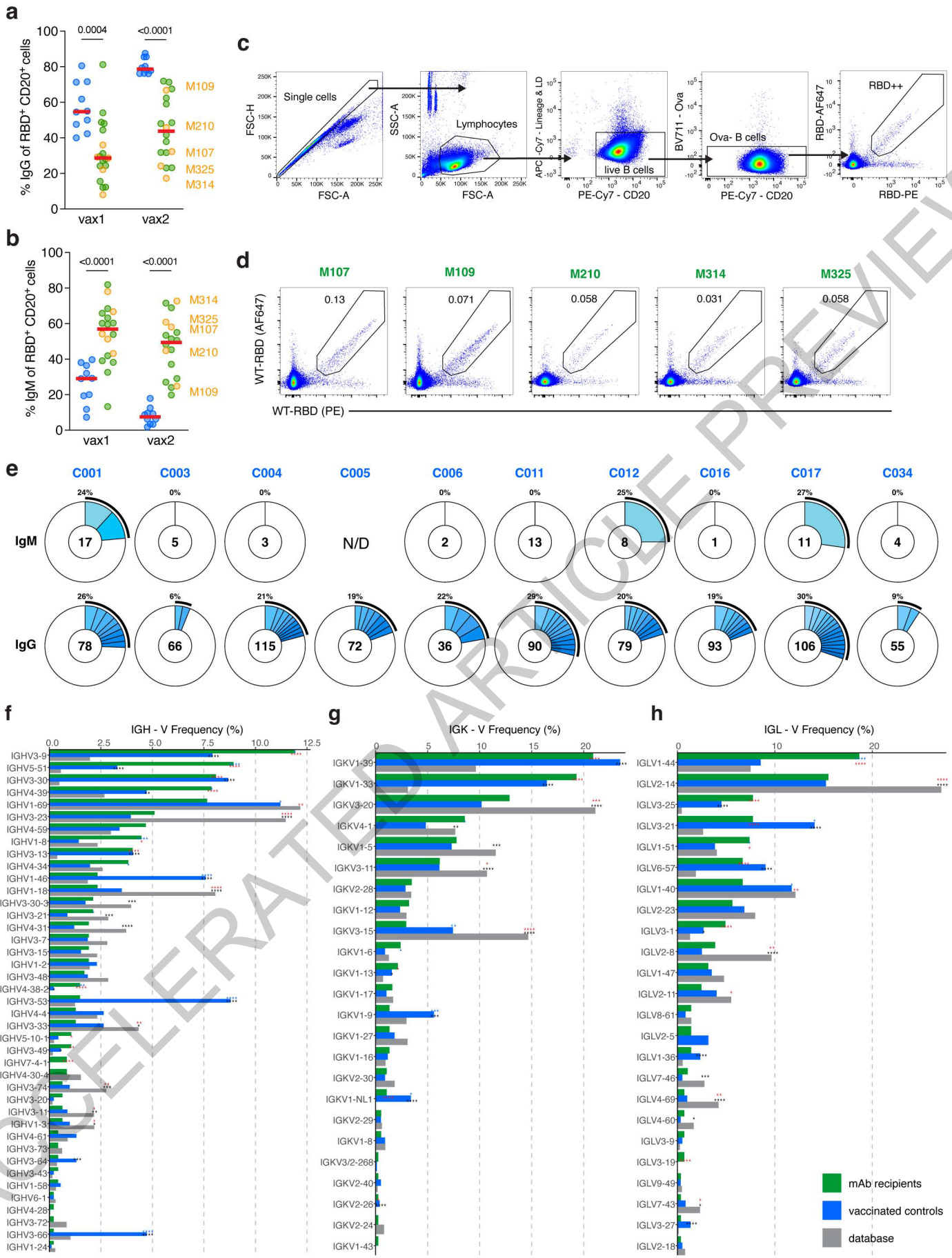

Extended Data Fig.4

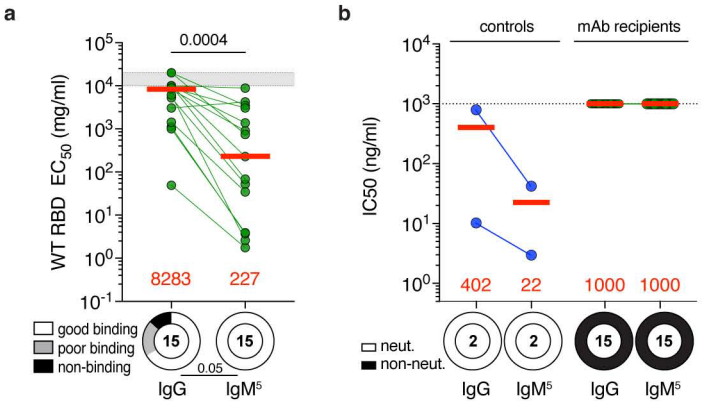

Extended Data Fig.5

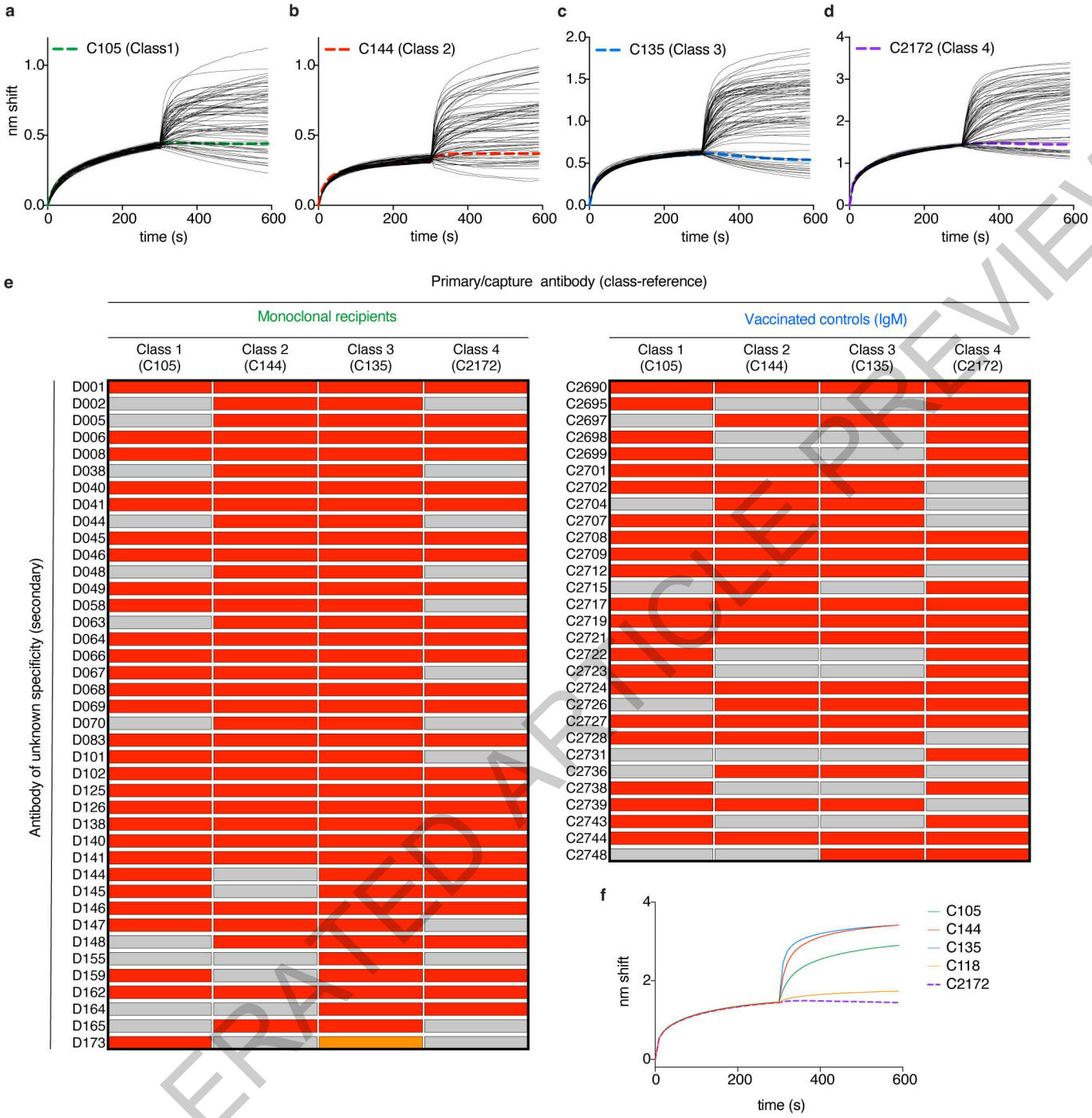

Extended Data Fig.6

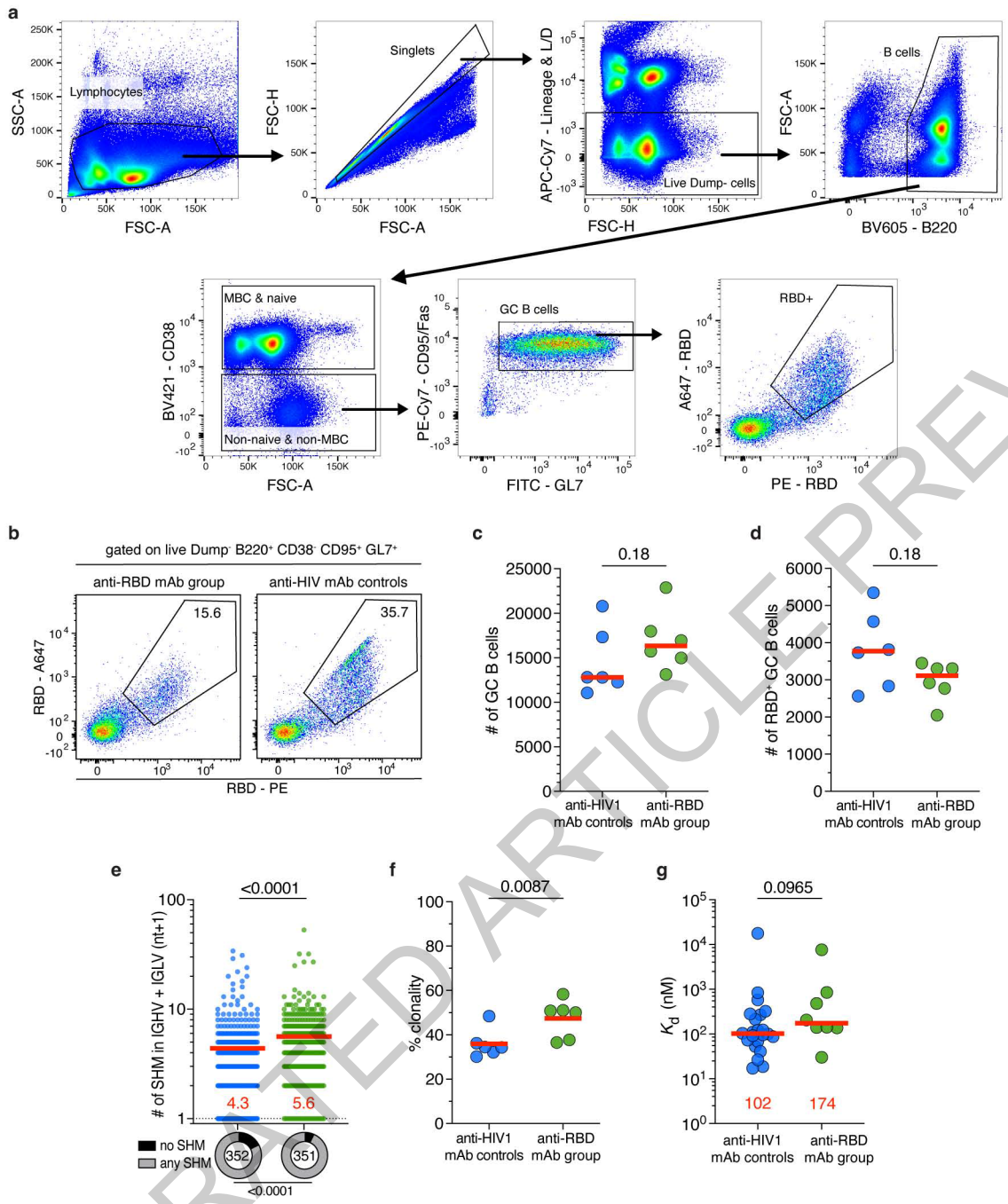

Extended Data Fig.7

nature portfolio

Corresponding author(s): Theodora Hatziioannou, Paul Bieniasz, Marina Caskey, Michel C. Nussenzweig

Last updated by author(s): Nov 17, 2022

Reporting Summary

Nature Portfolio wishes to improve the reproducibility of the work that we publish. This form provides structure for consistency and transparency in reporting. For further information on Nature Portfolio policies, see our Editorial Policies and the Editorial Policy Checklist.

Statistics

For all statistical analyses, confirm that the following items are present in the figure legend, table legend, main text, or Methods section.

n/a	Confirmed	
☐	☒	The exact sample size (*n*) for each experimental group/condition, given as a discrete number and unit of measurement
☐	☒	A statement on whether measurements were taken from distinct samples or whether the same sample was measured repeatedly
☐	☒	The statistical test(s) used AND whether they are one- or two-sided *Only common tests should be described solely by name; describe more complex techniques in the Methods section.*
☒	☐	A description of all covariates tested
☐	☒	A description of any assumptions or corrections, such as tests of normality and adjustment for multiple comparisons
☐	☒	A full description of the statistical parameters including central tendency (e.g. means) or other basic estimates (e.g. regression coefficient) AND variation (e.g. standard deviation) or associated estimates of uncertainty (e.g. confidence intervals)
☐	☒	For null hypothesis testing, the test statistic (e.g. *F*, *t*, *r*) with confidence intervals, effect sizes, degrees of freedom and *P* value noted *Give P values as exact values whenever suitable.*
☒	☐	For Bayesian analysis, information on the choice of priors and Markov chain Monte Carlo settings
☒	☐	For hierarchical and complex designs, identification of the appropriate level for tests and full reporting of outcomes
☐	☒	Estimates of effect sizes (e.g. Cohen's *d*, Pearson's *r*), indicating how they were calculated

Our web collection on statistics for biologists contains articles on many of the points above.

Software and code

Policy information about availability of computer code

Data collection	IRIS by iMedRIS version 11.01 for clinical data collection and management; BD FACSDiva Software Version 8.0.2 for flow sorting; ClarioStar Multimode reader by BMG Labtech (software version 5.70.R3) for neutralization assays; Omega 5.11 by BMG Labtech was used for ELISA Assays; Forte Bio Octet Data Acquisition software (version 11.1.3.25) for biolayer interferometry (BLI).
Data analysis	FlowJo 10.6.2 for FACS analysis; GraphPad Prism 9.3; Microsoft Excel 16.5.7; MacVector 17.5.4 for sequence analysis; Omega MARS V2.10 by BMG Labtech for luminometer/ELISA; Adobe Illustrator 2022; Geneious Prime (Versions 2020.1.2 and 2022.1.1); BBDuk (v38.93) for sequencing read processing, scripts and the data used to process antibody sequences are available on GitHub (https://github.com/stratust/igpipeline); Forte Bio Data Analysis HT (version 11.1.3.50) for BLI curve fitting.

For manuscripts utilizing custom algorithms or software that are central to the research but not yet described in published literature, software must be made available to editors and reviewers. We strongly encourage code deposition in a community repository (e.g. GitHub). See the Nature Portfolio guidelines for submitting code & software for further information.

Data

Policy information about availability of data

All manuscripts must include a data availability statement. This statement should provide the following information, where applicable:

- Accession codes, unique identifiers, or web links for publicly available datasets
- A description of any restrictions on data availability
- For clinical datasets or third party data, please ensure that the statement adheres to our policy

Data are provided in Supplementary Tables 1-6. The raw sequencing data associated with Figs. 2 and 4 have been deposited at Github (https://github.com/stratust/igpipeline/tree/igpipeline2_timepoint_v2). This study also uses data from "A Public Database of Memory and Naive B-Cell Receptor Sequences" (https://

doi.org/10.5061/dryad.35ks2), PDB (6VYB and 6NB6), cAb-Rep (https://cab-rep.c2b2.columbia.edu/), Sequence Read Archive (accession SRP010970), and from "High frequency of shared clonotypes in human B cell receptor repertoires" (https://doi.org/10.1038/s41586-019-0934-8).

Field-specific reporting

Please select the one below that is the best fit for your research. If you are not sure, read the appropriate sections before making your selection.

☒ Life sciences ☐ Behavioural & social sciences ☐ Ecological, evolutionary & environmental sciences

For a reference copy of the document with all sections, see nature.com/documents/nr-reporting-summary-flat.pdf

Life sciences study design

All studies must disclose on these points even when the disclosure is negative.

Sample size	No a priori sample size calculations were performed. The sample size of 18 individuals (mAb recipients) derives from practical reasons in that it is purely based on how many study participants of the phase 1 study (NCT04700163) elected to subsequently receive mRNA vaccination, remained SARS-CoV-2 infection-naive throughout the study observation period, and could be recruited for serial blood donations at the Rockefeller University Hospital in New York City. Individuals from the vaccinated controls (n=31) were not de novo recruited and have previously been reported on extensively (Cho et al., 2021 and Muecksch et al., 2022). Previous studies, such as the aforementioned Cho et al. and Muecksch et al. have also shown that a sample size of 10-30 individuals can yield representative biological insights as pertains to plasma antibody measurements and detailed molecular assays of memory B cells, thereby empirically validating our sample size selection. For further details about the human study subjects see Supplementary Tables 1 and 2. For mouse experiments (related to Fig. 4 and Ext. Data Fig. 7), the sample size of 6 individual animals per group was also not predetermined by statistical sample size calculations. Rather, it corresponds to a sample size that is generally accepted in the field, as it allows for rigorous hypothesis testing, simultaneously keeping the number of animals as small as possible while still being able to meet the scientific objectives (as per the 3R and ARRIVE guidelines).
Data exclusions	No data were excluded from the analysis.
Replication	All experiments successfully performed at least twice.
Randomization	This is not relevant as this is an observational study.
Blinding	This is not relevant as this is an observational study.

Reporting for specific materials, systems and methods

We require information from authors about some types of materials, experimental systems and methods used in many studies. Here, indicate whether each material, system or method listed is relevant to your study. If you are not sure if a list item applies to your research, read the appropriate section before selecting a response.

Materials & experimental systems

n/a	Involved in the study
☐	☒ Antibodies
☐	☒ Eukaryotic cell lines
☒	☐ Palaeontology and archaeology
☐	☒ Animals and other organisms
☐	☒ Human research participants
☐	☒ Clinical data
☒	☐ Dual use research of concern

Methods

n/a	Involved in the study
☒	☐ ChIP-seq
☐	☒ Flow cytometry
☒	☐ MRI-based neuroimaging

Antibodies

Antibodies used

1. Mouse anti-human CD20-PECy7 (BD Biosciences, 335793), clone L27
2. Mouse anti-human CD3-APC-eFluro 780 (Invitrogen, 47-0037-41), clone OKT3
3. Mouse anti-human CD8-APC-421eFluro 780 (Invitrogen, 47-0086-42), clone OKT8
4. Mouse anti-human CD16-APC-eFluro 780 (Invitrogen, 47-0168-41), clone eBioCB16
5. Mouse anti-human CD14-APC-eFluro 780 (Invitrogen, 47-0149-4), clone 61D3
6. Zombie NIR (BioLegend, 423105)
7. Mouse anti-human CD19-BV605 (Biolegend, 302244), clone HIB19
8. Mouse anti-human IgG-PECF594 (BD Bioscience, 562538), clone G18-145
9. Mouse anti-human IgM-AF700 (Biolegend, 314538), clone MHM-88
10. Peroxidase Goat anti-Human IgG Jackson Immuno Research 109-036-088
11. Peroxidase Goat anti-Human IgM Jackson Immuno Research 109-035-129

12. Rat anti-mouse T and -B cell activation antigen-FITC (BD Biosciences, 553666), clone GL7
13. Rat anti-CD38-PB (Biolegend, 102720), clone 90
14. Rat anti-mouse/human CD45R/B220-BV605 (Biolegend, 103244), clone RA3-6B2
15. Rat anti-mouse CD4-APC-eFluor780 (Invitrogen, 47-0042-82), clone RM4-5
16. Rat anti-mouse CD8a-APC-eFluor780 (Invitrogen, 47-0081-82), clone 53-6.7
17. Anti-mouse NK1.1-APC-eFluor780 (Invitrogen, 47-5941-82), clone PK136
18. Rat anti-mouse F4/80-APC-eFluor780 (Invitrogen, 47-4801-82), clone BM8
19. Armenian hamster anti-mouse CD95-PE-Cy7 (BD Biosciences, 557653), clone Jo2
20. Mouse anti-human CD38-BV421 (Biolegend, 303526), clone HIT2

Validation

All antibodies are commercially available and validated by manufacturers. Additional information can be found on the respective product websites listed below:
1. https://www.bdbiosciences.com/en-us/products/reagents/flow-cytometry-reagents/clinical-discovery-research/single-color-antibodies-ruo-gmp/pe-cy-7-mouse-anti-human-cd20.335793
2. https://https://www.biolegend.com/en-us/products/zombie-nir-fixable-viability-kit-8657www.thermofisher.com/antibody/product/CD3-Antibody-clone-OKT3-Monoclonal/47-0037-42
3. https://www.thermofisher.com/antibody/product/CD8a-Antibody-clone-OKT8-OKT-8-Monoclonal/47-0086-42
4. https://www.thermofisher.com/antibody/product/CD16-Antibody-clone-eBioCB16-CB16-Monoclonal/47-0168-42
5. https://www.thermofisher.com/antibody/product/CD14-Antibody-clone-61D3-Monoclonal/47-0149-42
6. https://www.biolegend.com/en-us/products/zombie-nir-fixable-viability-kit-8657
7. https://www.biolegend.com/en-us/products/brilliant-violet-605-anti-human-cd19-antibody-8483?GroupID=BLG5913
8. https://www.bdbiosciences.com/en-us/products/reagents/flow-cytometry-reagents/research-reagents/single-color-antibodies-ruo/pe-cf594-mouse-anti-human-igg.562538
9. https://www.biolegend.com/fr-lu/products/alexa-fluor-700-anti-human-igm-antibody-12507
10. https://www.jacksonimmuno.com/catalog/products/109-036-088
11. https://www.jacksonimmuno.com/catalog/products/109-035-129
12. https://www.bdbiosciences.com/en-us/products/reagents/flow-cytometry-reagents/research-reagents/single-color-antibodies-ruo/fitc-rat-anti-mouse-t-and-b-cell-activation-antigen.553666
13. https://www.biolegend.com/de-at/products/pacific-blue-anti-mouse-cd38-antibody-6652
14. https://www.biolegend.com/fr-fr/products/brilliant-violet-605-anti-mouse-human-cd45r-b220-antibody-7870
15. https://www.thermofisher.com/antibody/product/CD4-Antibody-clone-RM4-5-Monoclonal/47-0042-82
16. https://www.thermofisher.com/antibody/product/CD8a-Antibody-clone-53-6-7-Monoclonal/47-0081-82
17. https://www.thermofisher.com/antibody/product/NK1-1-Antibody-clone-PK136-Monoclonal/47-5941-82
18. https://www.thermofisher.com/antibody/product/F4-80-Antibody-clone-BM8-Monoclonal/47-4801-82
19. https://www.bdbiosciences.com/en-us/products/reagents/flow-cytometry-reagents/research-reagents/single-color-antibodies-ruo/pe-cy-7-hamster-anti-mouse-cd95.557653
20. https://www.biolegend.com/it-it/products/brilliant-violet-421-anti-human-cd38-antibody-7145

Eukaryotic cell lines

Policy information about cell lines

Cell line source(s)

293T (ATCC CRL-11268)
293T/ACE2* (generated in-house for Robbiani, D. et al. Nature 584, doi.org/10.1038/s41586-020-2456-9, and maintained since)
HT1080/ACE2.cl14 (generated in-house for Schmidt, F. et al. J Exp Med 217, doi:10.1084/jem.20201181, and maintained since)
Expi293F (GIBCO/Thermo Fisher, A14527)

Authentication

Not authenticated after purchase from ATCC and GIBCO/Thermo Fisher, respectively.

Mycoplasma contamination

All cell lines tested negative for mycoplasma contamination by Hoechst staining.

Commonly misidentified lines
(See ICLAC register)

No commonly misidentified cell lines were used.

Animals and other organisms

Policy information about studies involving animals; ARRIVE guidelines recommended for reporting animal research

Laboratory animals

C57BL/6 mice purchased from Jackson laboratory were used. All mice used were females between 6-12 weeks of age. Mice were housed at a temperature of 72 °F and humidity of 30–70% in a 12-h light/dark cycle with ad libitum access to food and water.

Wild animals

no usage of wild animals

Field-collected samples

none

Ethics oversight

All animal procedures and experiments were performed according to protocols approved by the Rockefeller University Institutional Animal Care and Use Committee (IACUC).

Note that full information on the approval of the study protocol must also be provided in the manuscript.

Human research participants

Policy information about studies involving human research participants

Population characteristics	Participants in the monoclonal recipient group were healthy volunteers who had previously received a single dose of a combination of C144-LS and C135-LS, two human IgG1 neutralizing anti-RBD monoclonal antibodies (first characterized in Robbiani et al., 2020), in a phase 1, first-in-humans study to assess the safety and tolerability as well as the pharmacokinetics of the two antibodies (NCT04700163), and who subsequently got vaccinated with the initial two-dose regimen of either the Moderna (mRNA-1273) or Pfizer-BioNTech (BNT162b2) mRNA vaccines against the wildtype (Wuhan-Hu-1) strain of the severe acute respiratory syndrome coronavirus 2 (SARS-CoV-2). Of note, vaccinations were at the discretion of each individual participant and their health care providers and not part of our study design, which was purely observational in nature. Particpants were 43 (24-64) years old (median (range)), 5 out of 18 participants were female. 6 participants received the Moderna (mRNA-1273) and 12 received the Pfizer-BioNTech (BNT162b2) vaccine. Participants in the vaccinated controls group were not de novo recruited for this study and we defer to Supplementary Information Tables S1 and S2, as well as Cho et al., 2021 and Muecksch et al., 2022 for more details.
Recruitment	Recruitment of individuals into the antibody recipient group of this study was pragmatic, in that all eligible participants (no history of SARS-CoV-2 infection, having received active agent C135-LS and C144-LS and not placebo, subsequent vaccination with 2 doses of either the Moderna (Spikevax, mRNA-1273) or Pfizer-BioNTech (Comirnaty, BNT162b2) mRNA vaccines against the wildtype (Wuhan-Hu-1) strain) of the phase 1 clinical trial (NCT04700163) were offered enrollment in the observational study reported on herein. As with all human subjects research based on healthy volunteers, the study cohort composition may be biased toward individuals with more access to health- and science-related resources. However, due to the direct linkage of this observational study to the phase 1 trial (NCT04700163), additional biases, such as self-selection bias, are unlikely. No further recruitment efforts were undertaken, as the control group was not de novo recruited for this study. A detailed description of their recruitment can be found in Cho et al., 2021 and Muecksch et al., 2022.
Ethics oversight	The study was performed in compliance with all relevant ethical regulations and the protocols (CGA-1015 and DRO-1006) for studies with human participants were approved by the Institutional Review Board of the Rockefeller University.

Note that full information on the approval of the study protocol must also be provided in the manuscript.

Clinical data

Policy information about clinical studies

All manuscripts should comply with the ICMJE guidelines for publication of clinical research and a completed CONSORT checklist must be included with all submissions.

Clinical trial registration	NCT04700163
Study protocol	The study protocol can be accessed under clinicaltrials.gov (https://clinicaltrials.gov/ct2/show/NCT04700163)
Data collection	The study "A Phase 1, Open Label, Dose-escalation Study of the Safety and Pharmacokinetics of a Combination of Two Anti-SARS-CoV-2 mAbs (C144-LS and C135-LS) in Healthy Volunteers" (NCT04700163) was conducted at The Rockefeller University between January 11, 2021 and February 2, 2022.
Outcomes	NCT04700163 was conducted to assess the safety and tolerability, as well as the pharmacokinetics of C144-LS and C135-LS, with adverse events and phamacokinetic properties of the infused antibodies as its primary and secondary outcomes. However, the study presented here explicitly does not report on the pre-defined endpoints of NCT04700163. Instead, the data presented in this manuscript merely represents an observational study of the immune response to vaccination in participants of NCT04700163, which does not constitute a pre-specified outcome of NCT04700163.

Flow Cytometry

Plots

Confirm that:

☒ The axis labels state the marker and fluorochrome used (e.g. CD4-FITC).

☒ The axis scales are clearly visible. Include numbers along axes only for bottom left plot of group (a 'group' is an analysis of identical markers).

☒ All plots are contour plots with outliers or pseudocolor plots.

☒ A numerical value for number of cells or percentage (with statistics) is provided.

Methodology

Sample preparation	For human samples, whole blood samples were obtained from study participants recruited through Rockefeller University Hospital. Peripheral blood mononuclear cells (PBMCs) were separated by Ficoll gradient centrifugation. Prior to sorting, PBMCs were enriched for B cells using a Miltenyi Biotech pan B cell isolation kit (cat. no. 130-101-638) and LS columns (cat. no. 130-042-401).

For mouse experiments, popliteal lymph nodes from mice 11 days after immunization were isolated and collected in FACS buffer (1x PBS, 2% FBS, 2 mM EDTA). Single cell suspensions of the pooled popliteal lymph node samples from each respective mouse were subsequently processed as described.

Instrument

FACS Aria III (Becton Dickinson), BD FACSymphony S6 (Becton Dickinson)

Software

BD FACSDiva Software Version 8.0.2 and FlowJo 10.6.2

Cell population abundance

For the human experiments, sorting efficiency ranged from 40% to 80%. This is calculated based on the number of antibody sequences that could be successfully PCR-amplified from single-sorted cells from each donor using either IgM or IgG heavy chain-specific primers (see Robbiani et al., 2020 and Wang et al., 2020) in conjunction with IgK and IgL-specific light chain primers.

For the mouse experiments, GC B cell abundance was not a limiting factor for cell sorting. Sorting efficiencies (based on the same calculation as above) were slightly lower (between 30 to 80%), with the notable difference that only IgK-specific light chain primers were used.

Gating strategy

For human experiments, cells were first gated for single cells in FSC-A versus FSC-H, and then for lymphocytes in FSC-A (x-axis) versus SSC-A (y-axis). We then selected for either CD20+ (cell sorting) or CD19+CD20+ (flow-cytometric phenotyping) and Dump- B Cells in dump (anti-CD3-eFluro 780, anti-CD16-eFluro 780, anti-CD8-eFluro 780, anti-CD14-eFluro 780, Zombie NIR) versus CD20 (anti-CD20-PE-Cy7) or versus CD19 (anti-CD19-BV605); dump-negative was considered to be signal less than 1200, CD19-positive was taken to be signal greater than 1000, and CD20-positive was taken to be signal greater than 500. We then gated for Ova- B cells in CD20 versus Ova-BV711; Ova-negative was considered to be all cells with signal less than 1200 (flow-cytometry) or 300 (cell sorting). We selected for Sars-CoV-2 RBD double-positive cells in RBD-PE versus RBD-AlexaFluor 647; this gate was made along the 45° diagonal, above 1000 (flow-cytometry) or 500 (cell-sorting) on both axes. IgG+ (IgG-PECF594) versus IgM+ (IgM-AF700) cells among RBD dual-labelled cells were gated using mutually exclusive gates with signals above 1000 for each.

For mouse experiments, gating was as detailed in Ext. Data Fig. 7a. Briefly, single live cells were gated to only include cells negative for staining with anti-CD4-APC-eFluor780, anti-CD8a-APC-eFluor780, anti-NK1.1-APC-eFluor780, anti-F4/80-APC-eFluor780 and and Zombie NIR to exclude dead and irrelevant cell populations. Next, cells positive for staining with anti-CD45R/B220-BV605 were considered B cells. B cells with MFIs <1000 for staining with anti-CD38-PB/BV421 and positive for staining with anti-GL7-FITC and anti-CD95-PE-Cy7 were considered GC B cells. Among those, cells with MFIs higher than 500 for RBD-A647 and 1000 for RBD-PE were deemed RBD-binding. Cell sorting was done on cells in the GC B cell gate agnostic of binding to RBD. RBD-binding status of single-sorted cells was established post-factum through index sorting data, using the same gating as in Ext. Data Fig 7a and b.

☒ Tick this box to confirm that a figure exemplifying the gating strategy is provided in the Supplementary Information.